The Pennsylvania State University

Electrical Engineering Department

University Park, Pennsylvania 16802

SECONDARY ELECTRON EMISSION FROM A DIELECTRIC FILM SUBJECTED TO AN ELECTRIC FIELD

Technical Report

NASA Grant No. NSG-3097

Nguyên Quôć-Nguyên

November 1977

The Pennsylvania State University

The Graduate School

Department of Electrical Engineering

Secondary Electron Emission from a Dielectric Film Subjected to an Electric Field

A Thesis in

Electrical Engineering

by

Nguyễn Quốc-Nguyên

Submitted in Partial Fulfillment
of the Requirements
for the Degree of

Master of Science

November 1977

ABSTRACT

An electric field in the range of [0.3, 3.3] kV/mm is created normal to a thin-film FEP Teflon sample which accumulates potential of up to 8.8, 13.7 or 18.3 kV when exposed to an electron beam having energy of 10.0, 15.0 or 20.0 kV, respectively. It is found that the secondary electron emission from the charged sample varies with field. The threshold voltage, at which the secondary electron emission coefficient σ is unity, drops down from a low field value of 13.73 kV to a high field value of 13.11 kV for a 15.0 kV beam. The maximum value of σ measured at some primary beam voltage larger than the threshold falls off from 2.8 to 1.9. The beams are perpendicular to the sample's surface, i.e., parallel to the field.

The established charge on the sample decays steeply near the edge of a metal-dielectric interface. A calculation based on the potential shows a precipitous gradient of about 10 kV/mm being at the border. This gradient encourages the secondary electron emission as a charge transport mechanism by which stable charge distribution may be established near the interface.

A computational technique has been developed that generates equipotential lines or contours and field vectors above a plane where potential is known. Furthermore, the utilization of conformal transformations allows the extension of the technique to configurations which map into

a plane. Nevertheless, it is assumed that the potential on the surface varies as a function of only one variable and that the equipotential lines or contours must start from the surface. Resulting lines or contours and vectors are two dimensional.

TABLE OF CONTENTS

LIST OF TABLES

LIST OF FIGURES

ACKNOWLEDGMENTS

The author is grateful to Dr. James W. Robinson, who supervised this work with invaluable instructions and enthusiasm. He is indebted to Dr. John L. Brown, Jr. from whom he had learned much. He extends his thanks to Dr. David R. Voltmer, who was willing to read and comment on these pages. Finally, another aspect is that financial support from the National Aeronautics and Space Administration under Grant NSG-3097 was greatly appreciated.

I. INTRODUCTION AND SURVEYS

The foci of these experiments are charge accumulation and secondary-electron emission from a dielectric film in the region near a metal-dielectric interface which is irradiated by an electron beam. First of all, the charge (potential) distribution of that region was measured. Accordingly, an electric field pattern could be plotted from this information via electrostatic theory and computer programming. Then, the experiments examined the influence of field, both the computed field and an externally applied field, upon secondary-electron emission.

Although we could not think of an effective way of measuring the secondary-electron emission near the interface, a qualitative attempt to deduce its behavior is made at the end of this report. The deduction characterizes it in terms of the accumulated charge (potential) the calculated, immoderate field in that border, and in terms of the measured emissions at the central region where the undeflected beam is normal to the sample's surface.

Most of the experiments were with a FEP-Teflon sample, having thickness of 0.127 mm and one-side coated with silver inconel. This is one of the materials used to construct spacecraft. We also did some tests with 0.051-thick-Teflon sheet as well with aluminized Kapton which has properties similar to the Teflon. However, the thinner sheet of Teflon and the Kapton were found to be less suitable because of

leakages of electrons for high energy beams. In a vacuum chamber, having pressure of about 10^{-5} Torr, the sample is mounted under an aluminum aperture and exposed to an electron beam with a kinetic energy of 10, 15, or 20 keV. The aperture not only defines the exposed area of the sample but also creates the metal-dielectric interface. A literature search of work done previously on the secondary-electron emission is briefly summarized in the succeeding paragraphs.

The phenomenon of secondary-electron emission was discovered by Austin and Starke in 1902 [1]. Austin and Starke were studying the reflection of cathode rays from metal surfaces and found that the metal target was able to emit a larger number of electrons than it was receiving. The striking electrons are called primary electrons and the liberated electrons are called secondary electrons. It is a complicated pheonomenon involving many different and interelated processes taking place at the target when its surface is irradiated by primary-beam kinetic electrons. There are three groups of secondary electrons emitted from the surface of a target: primary electrons reflected elastically, primary electrons reflected inelastically, and true secondary electrons. The energies of the secondary electrons released by a material vary from zero to the energy of the primary beam, and a typical energy distribution is shown in Fig. (I-1) for silver (solid) bombarded with electrons having energy slightly above 150 eV [2]. N(E) is the relative

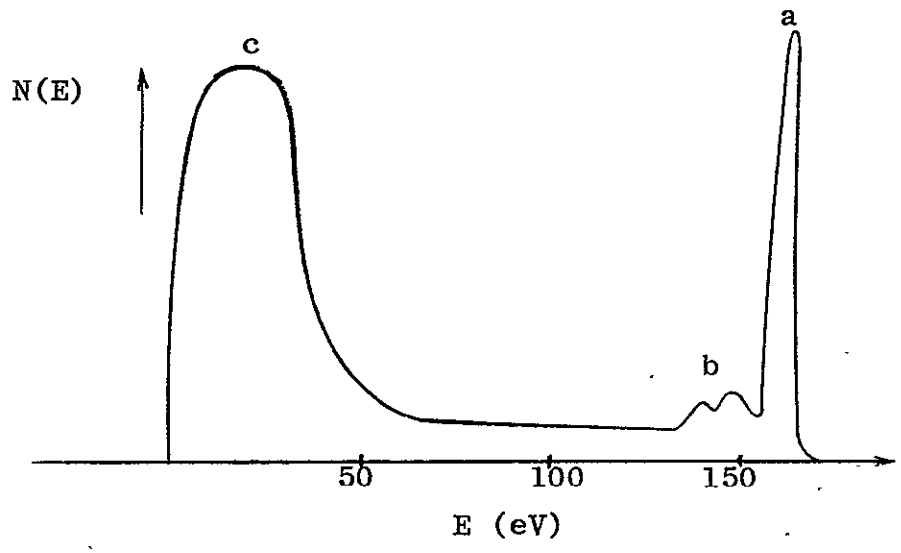

Figure (I-1) Energy distribution of secondary electrons.

number of secondary electrons with energy E. There are three peaks in this distribution, denoted by a, b, and c, corresponding to the three types of emission: elastic, inelastic, and true secondary electrons, respectively.

In application, people are often interested in the ratio of a number of primary electron over a number of secondary electron no matter to which group the secondary electrons belong. This ratio, namely secondary electron emission coefficient σ, may take any value from 0.5 for some metals to nearly 4.0 for some dielectrics. It depends on the cleanness and temperature of the surface, on the angle of incident electrons, on the work function of material, and of course, on the primary beam energy E_p. Cleanness, however, does not cause any serious problem if the medium is kept at a sufficiently low pressure. It will be ignored here.

The fact that the secondary emission from metals is practically independent of temperature indicates that the main process of energy loss is by interaction with the free electrons and not with lattice vibrations, which would certainly be temperature sensitive. In insulators interaction of the secondaries with the lattice vibrations becomes significant, and this accounts for the reduction of secondary emission with increasing temperature observed in these materials. The coefficient σ is high in insulators. If the primary beam is incident at an angle θ to the normal to the surface, the secondary emission at low primary energy is very similar to the value for normal incidence; but at higher energy σ increases as θ is increased. The primary energy E_{pmax} at which σ has its maximum value also increases as θ increases [2].

One might expect to find a high yield of secondary electrons from metals with a low work function, but this is not in accordance with the experimental results. McKay [3] has plotted σ_{max} as a function of the work function of different metals and the result is just the contrary, namely a high work function corresponds to a high σ_{max}. McKay observes rightly that the work function itself plays a relatively minor role in determining the secondary emission yield, but other physical properties such as the density are probably of more importance. When primary beam energy E_p is small the work function is apparently a governing factor [4].

It is unnecessary to emphasize that the development of a theory of secondary-electron emission is no simple task. Various authors have made their contributions. Some theories are more or less phenomenological; others are based on a model, either classical, or the wave mechanical model of Bloch. The following paragraphs summarize some of their investigations.

According to Bruining [5], the liberation of secondary electrons occurs by the transfer of energy from the primary electrons to the electrons of the lattice. The behavior of the primary electron is determined by its energy loss as a function of penetration depth, its absorption, and scattering. The secondary electrons are scattered, and before reaching the surface a fraction will be lost by absorption. Moreover, the work function has to be overcome before an emission is possible. He displayed an equation representing a universal curved based on theoretical considerations only,

$$\frac{\sigma}{\sigma_{max}} = 1.85\ F\left[\frac{0.92E_p}{E_{pmax}}\right] , \qquad (I\text{-}1)$$

where

$$F(r) = e^{-r^2}\int_0^r e^{y^2}dy \ , \text{ and } \ r = E_p\sqrt{\frac{\alpha}{a}}$$

with α and a depending on material.

It is striking that a universal curve, applicable to metals, can be found in actual fact as shown in Fig. (I-2).

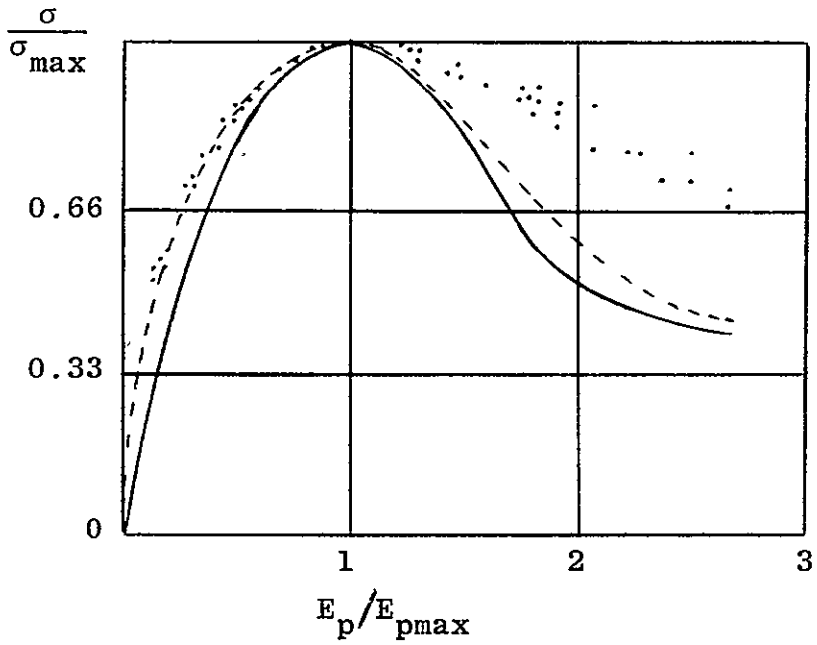

Figure (I-2) Universal σ versus E_p curve: full line according to Baroody [7], Eqn. (I-1); dotted line according to Jonker [6], Eqn. (I-2); the points represent measured data.

We assume with Jonker [6] that the secondary electrons are equally distributed in space at the point of origination. Then Eq. (I-1) must be modified to read:

$$\frac{\sigma}{\sigma_{max}} = \frac{1}{0.33}\, f\left(0.71\, \frac{E_p}{E_{pmax}}\right) , \qquad (I\text{-}2)$$

where

$$f(r) = \int_0^1 dz\, \exp(-r^2/z) z^{\frac{1}{2}} \int_0^{\sqrt{r^2/z}} dy\, \exp(y^2), \text{ and } r = E_p \sqrt{\frac{\alpha}{a}}$$

The smooth curve in Fig. (I-2) must be replaced by the broken curve, and thus is somewhat better accord with the observed data.

Second mention will be given to the theories of Kadyschevitz [8] and later Baroody [9], who used the Sommerfeld model and calculated the energy transfer to the conduction electrons along classical lines. Baroody did not follow his model consistently; he could have derived the relation between penetration depth and energy of the primary electron, but instead assumed Whiddington's law. Nevertheless Baroody made an important contribution to existing theories which has been discussed.

Quantum-mechanical theories have been developed by Frohlich [10], Woldridge [11] and Dekker and van Der Ziel [12]. These authors used Bloch model for metals and considered the collision of a single primary electron with a single metal electron. They paid special attention to the direction of the momentum transferred; thus in their model the emission of entirely free electron is impossible, since this would be contrary to the law of conservation of momentum.

The most recent search on dielectric properties by Wall, Burke and Frederickson [13] states that although not all incident electron energies of interest have been covered for all materials, sound theoretical and semiempirical relationships have been developed that can be used to extend the available data. An example of such a relationship is the "universal secondary emission curve." It is given by:

$$\frac{\sigma}{\sigma_{max}} = \frac{X_{max}^{1-n}}{g_n(X_{max})} \left(\frac{E_p}{E_{pmax}}\right)^{1-n} , \qquad (I-3)$$

where $g_n(X) = [1-\exp(-X)^n]/X^{n-1}$ with X_{max} is the value of X for g_n to be maximal. For a given material, X_{max} and n must be determined numerically to fit the available data. Most measured values of the secondary emission coefficient can be fit to the universal curve. In fact, if data is found that cannot be fit to the curve, there were probably errors made during the measurements. Fig. (I-3) shows secondary emission data for Teflon taken from Matskevich [14] fitted to the universal curve. The data was taken from a plot in the paper and deviations of some points from the curve are probably due as much to reading the plot as to experimental error.

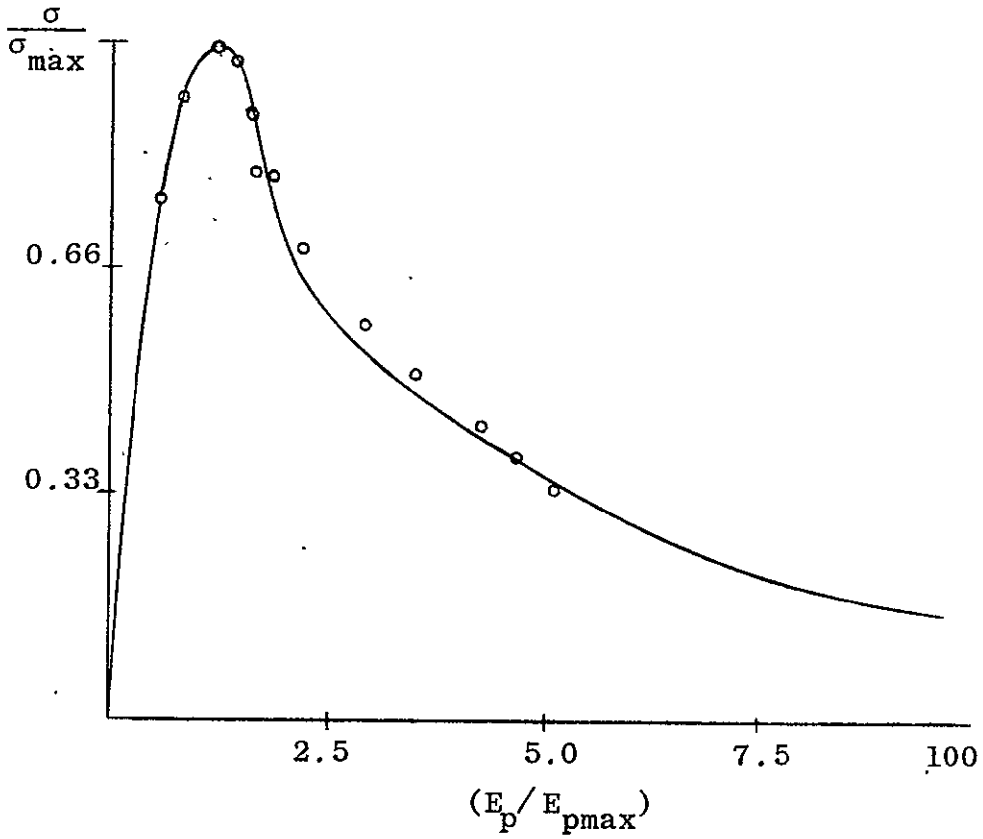

Figure (I-3) o points are measured data for Teflon with $\sigma_{max}=2.21$, $E_{pmax}=0.4$ keV. Solid line is the curve yielded from Eqn.(I-3) with n=1.725.

For electron energies above about 0.5 keV, the following empirical relationship holds well:

$$\sigma = KE^{-m} \quad , \tag{I-4}$$

where K and m are constants. For most organics m is found to be about 0.725 and K depends on the specific material. The angular dependence of secondary emission follows the semiempirical relation:

$$\sigma_\theta = \sigma_o \exp[C(1-\cos\theta)] \quad , \tag{I-5}$$

where

θ = angle of incidence of electrons with respect to the surface normal

σ_o = secondary emission coefficient at normal incidence

σ_θ = secondary emission coefficient for electrons incident at angle θ.

The constant C is determined empirically. For most polymers, C is approximately two.

Because of its practical applications, secondary emission has long been a subject of exploration. As a result, a considerable volume of data exists covering many materials including metals and insulators. However, no theory has yet been found which satisfactorily covers all the observed phenomena. In as many books and publications as we could find, most of the authors deal with an

anode-cathode construction where the anode is a target, or with an arrangement where secondary electrons are liberated from the material itself by bombardment. The thing which we would like to point out is that we are studying the subject of secondary-electron emission from a different view. The measurements are accomplished with a sample having an accumulated charge of electrons. They, therefore, include the effects of the accumulated electrons on the surface and the intrinsic electrons of the material. The second difference is the existence of an excessive field in the medium. Moreover, due to the unequally-distributed charge from the edge of the interface to the center of the charged sample the space above the sample possesses an inherently nonuniform field. A closely coordinated report [15] by Robinson concentrates on the measurements of specimen charging and flashovers.

Since apparatus and methods of measurement play a key role in attacking the goal, the descriptive Chapter II is for them. We then pay attention to the principal interests of this work, Chapter III and IV, field calculations and secondary-electron emission in the presence of field. In Chapter III, we introduce a generalized-analytic-computational technique of equipotential and field mapping which are applicable to numerous electrostatic problems. Chapter IV is a mathematical formalism associated with the method of converting the outputs of the measurements, graphs on a recording chart, into a meaningful term, the

secondary-electron emission coefficient. It also displays plots of the coefficient versus beam energy and the coefficient versus estimated field. Chapter V is merely a review and comments on important points in the preceding chapters. For clarifications, the appendix contains materials such as proofs of some expressions, tabulated formulae, and the computer program which was written for calculating equipotential contours.

II. DESCRIPTION OF APPARATUS AND METHODS OF MEASUREMENT

Apparatus should be appropriate for methods and vice versa to accomplish the objectives. Two major methods shall be applied, one being duplicated from Robinson's work [16], the other being a qualified modification of the first. Some pieces of apparatus were available on the market while some others were assembled in our laboratory to meet the methods' requirements. We tend to describe the performance of the apparatus rather than their dimensions which, not being crucial in the measurements, will be omitted for simplicity.

A. Apparatus

Apparatus is divided into three groups of equipment: the vacuum system itself, the apparatus inside, and the instruments outside of the vacuum.

1. The vacuum system

A chamber covered with a stainless steel bell jar having a diameter of 44.5 cm, and a height of 73.60 cm, is evacuated by a turbomolecular pump to a base pressure of 10^{-6} Torr. The conventional vacuum system is equipped with an ionization gauge, a controllable leak, and assorted electrical and mechanical feedthroughs Fe1, Fm1, and Fm2 in the base plate as shown in Fig. (II-1). Voltage feedthroughs Fe2 for the electron source are on the side of the bell jar. A glass window at the middle of the bell jar offers a view of the interior.

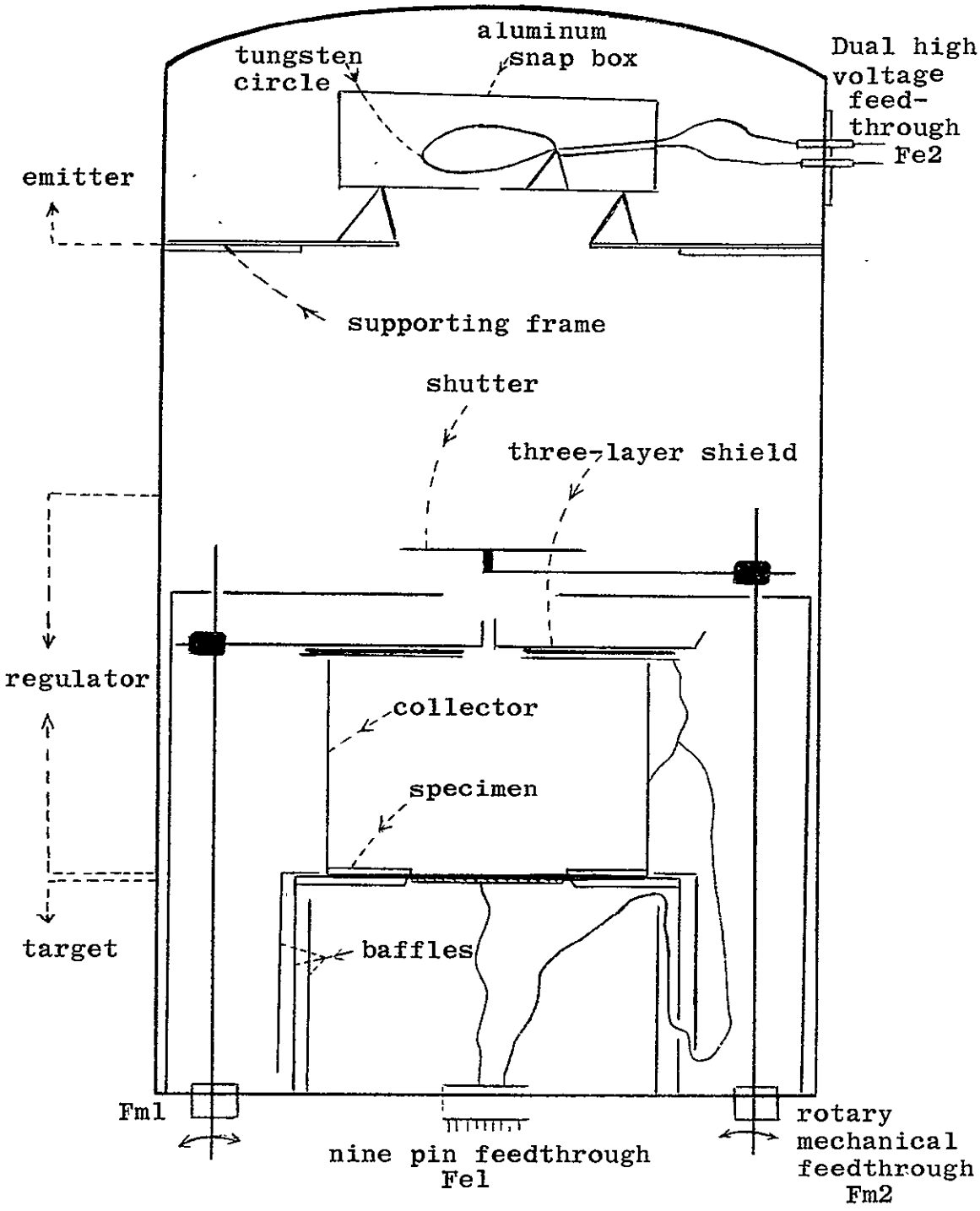

Figure (II-1) Internal arrangement of the chamber has three constituents: an emitter, a regulator, and a target.

2. Inside the bell jar

There are three main components in the chamber: an emitter, a target and a regulator as shown in Fig. (II-1). The emitter is an electron source made of a 3.80 cm diameter circle of 10 mil tungsten in an aluminum snap box, as shown in Fig. (II-2). Through the tungsten circle runs a 4-6 A current provided by the secondary coil of an isolation transformer where the primary voltage is adjustable up to 120 volts.

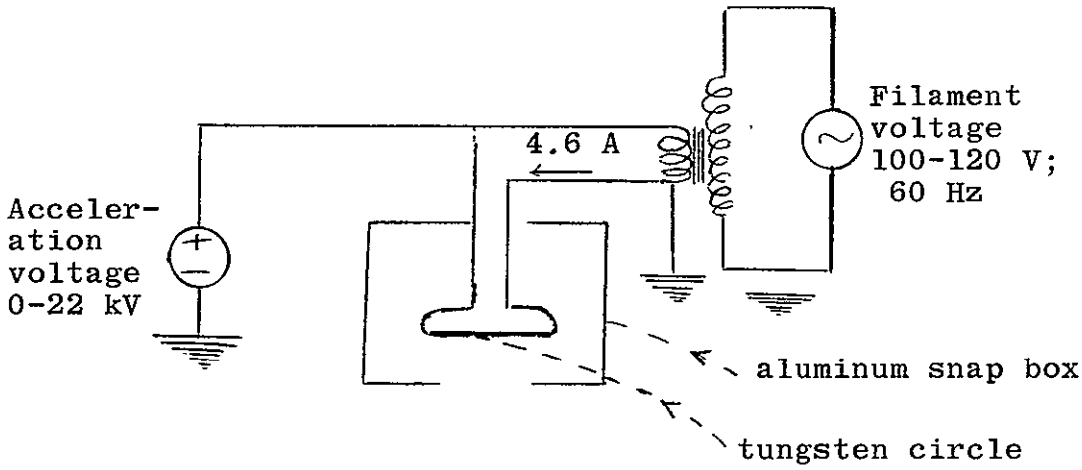

Figure (II-2) Structure of the emitter.

The target essentially includes a specimen and three baffles. The specimen is mounted as shown in Fig. (II-1) on an eight-inch diameter aluminum disk which has a slot. Electrical contacts from the dielectric sample to the feed-throughs Fel underneath are established through this slot. The specimen defines the exposed area of the sample via an

aluminum aperture plate placed on top and creates a metal-dielectric interface. (Sample preparations shall be described in Section B.) Below the specimen, the baffles, surrounding the feedthroughs like curtains, prevent free electrons from striking the electrical terminals under the sample.

The regulator consists of five elements: a collector, a screen, a shield, a baffle, and a shutter.

a) The collector is an aluminum cylinder, having a radius of 51.5 mm and a height of 51.5 mm, being mounted on the aperture plate. This assembly is isolated from the grounding disk by the sample. Its function is to collect secondary electrons emitted from the sample and it is connected to an electrometer via the feedthrough Fel. The dimensions of the collector were chosen so that it would not disturb the charge accumulation on the sample.

b) The screen with transparency of 85%, a 304-stainless steel meshes made of 25.4 μm-diameter wire having 0.2286 mm gap between each two of them, is hung above the sample and connected to the collector which is grounded through the electrometer to create a field between it and the charged sample.

c) The shield is used with the collector. It is a three-layer triangle, shown in Fig. (II-3), attached to the rotary mechanical feedthrough Fml.

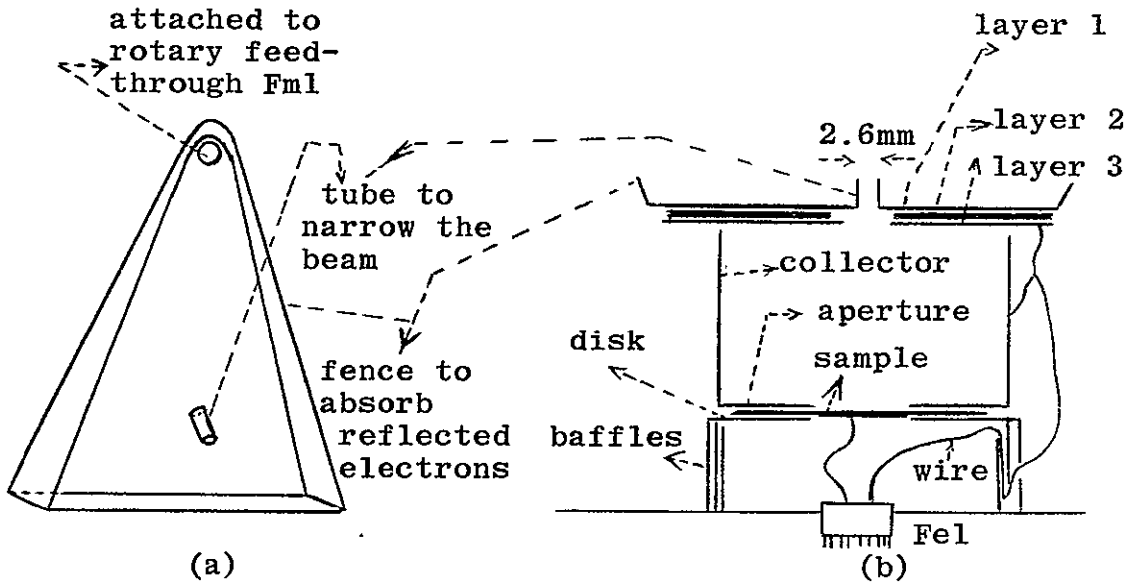

Figure (II-3) a. Top view of the shield
b. Cross-section of the shield, the collector and the target (thickness of the sample is exaggerated).

Layer 1 is a grounded triangular sheet of aluminum on which a 2.6 mm inner diameter tube is positioned in such a way that only electrons whose trajectories are straight through the tube can reach the sample. Its sides are bent up to absorb the reflected electrons. Layer 2 is a dielectric sheet to separate layer 3 from the grounding layer 1. Layer 3 is a cap for the collector. It captures secondary electrons released from the sample which do not strike the collector. It is connected to the collector with a flexible wire.

None of the dielectric surfaces of the shield are exposed to the beam or to secondary electrons. Otherwise, they would accumulate charge. The shield slides on the collector so that the tube projects a locus across the

sample. It can be slidden sufficiently far to completely expose the sample under the beam through the large hole on the baffle.

d) The baffle is grounded and it prevents free electrons from striking the collector.

e) The shutter is attached to the mechanical rotary feedthrough Fm2. It covers the tube, and the large hole on the baffle as well, therefore, eclipsing the sample when necessary.

All the items are cleaned chemically with trichlorolene and methanol before being put into the vacuum so that low pressure could be attained with a short pumping time. The sample, however, was not cleaned chemically, because chemicals might change its properties.

3. Outside the bell jar

Equipment outside the chamber consists of power supplies to the inputs, Fe2, and meters to measure the outputs, Fe1.

Two power supplies are needed. One provides an acceleration voltage to the snap box shown in Fig. (II-2) in the range of [0.0, 22.0] Kilovolt d.c. and it biases the filament by the same amount. It is a partial supply for the emitter through feedthrough Fe2. The other is a reference voltage in the range of the acceleration voltage. Reference and acceleration voltages are two terminals of a voltmeter where the difference is readable as low as 20.0

volt. The reference voltage is useful when we want to alter accelerating voltage by a small amount.

Two electrometers designated M1 and M2 are used to register the responses of the dielectric sample and to amplify them in terms of coulombs, volts, or amperes. They are connected to the sample and the collector via Fel. A dual-channel recorder plots the amplified signals from M1 and M2 and its outputs are graphs on a recording chart. The electrometers and the recorder are calibrated adequately so that quantitative data can be taken from the graphs.

B. Methods of measurement

Two methods were employed. They are different in sample preparations, in equipment and in procedure.

1. Preparation of samples

Most of the work is with 5 mil FEP Teflon sheet which had been coated on one side with silver and then inconel. The material is mounted with the uncoated side exposed to an electron beam and the coating itself maintained at a virtual ground potential. The goal is to isolate an exposed region where we can do the measurements. The metal-film ground plane is cut into segments by an electrical discharge as illustrated in Fig. (II-4). Ref. [16] is the origin of this fabrication. Each segment of the underlying ground plane was grounded by its own separate connecting wire. Measurements of charge (or current) were made by grounding a particular segment through an electrometer which measures a

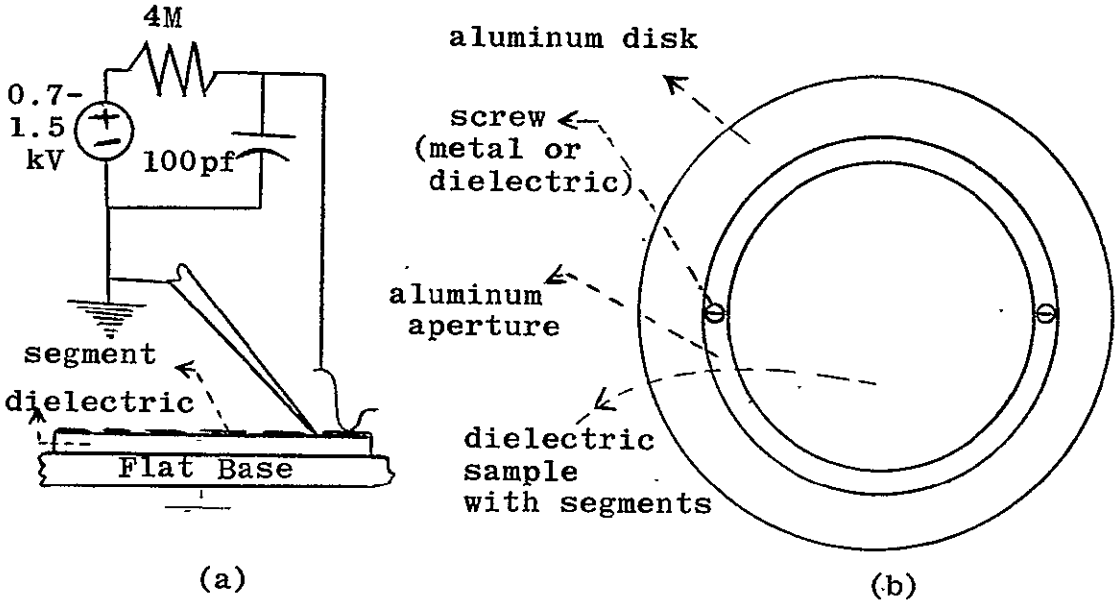

Figure (II-4) a. A scheme to segment a metal coating of a dielectric sheet
b. Top view of the specimen and the disk.

charge (or induced current) while maintaining a virtual ground. Electrical connections to segments were constructed by bonding #32 copper wires to the segments with silver-filled epoxy. These wires lead to nearby ceramic insulated binding posts from which connections can be made easily. Two kinds of samples are fabricated to go with the two specific methods. Sample Sa1 has many small-rectangular segments whose top view was shown in Fig. (II-4) and whose cross-section is shown in Fig. (II-5). Sample Sa2 has one circular segment for which the isolated ground region through the electrometer equals the area exposed under the beam (when the shield and the shutter are turned aside).

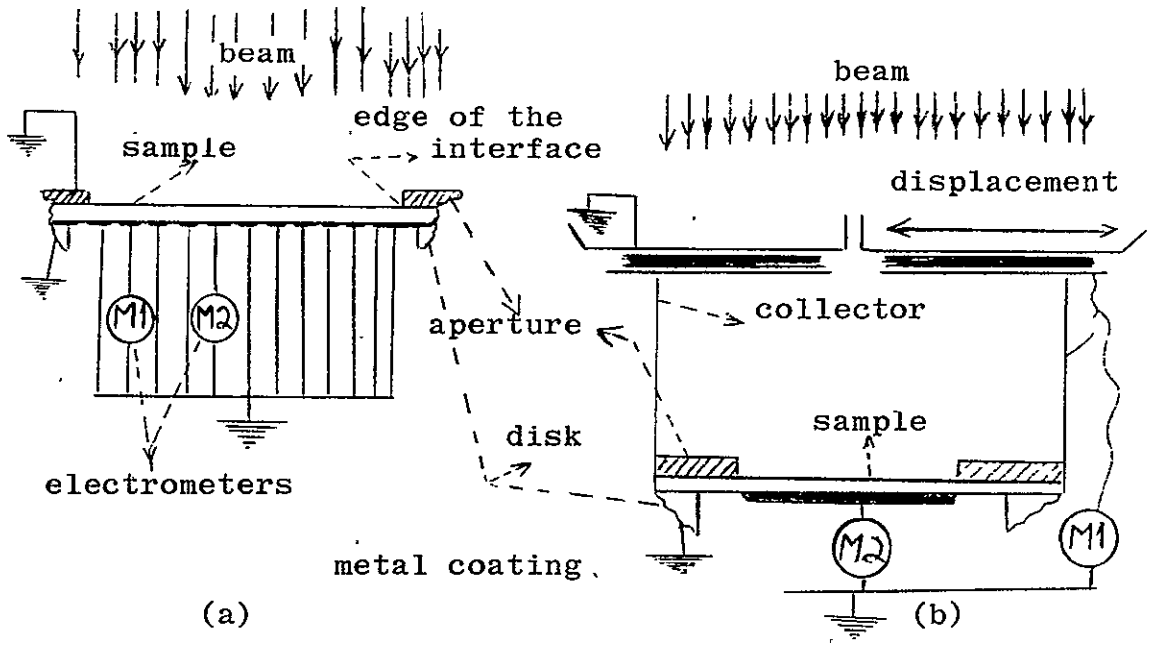

Figure (II-5) Two samples shown with exaggerated thickness.
a. cross-section of Sa1. Charges on two segments are measured while other segments are grounded
b. cross-section of the shield, the collector and the specimen with Sa2 in action.

2. Method Number 1

The objective of this method [16] is to gain a charge (voltage) distribution across a dielectric sample when it is being irradiated by a certain primary beam having a voltage of 5, 10, or 20 kV. We measure the charge q_i on each isolated segment from the edge of the middle to the sample as well capacitance c_i of each. Then, the voltage is given by $v_i = q_i/c_i$ for the center point of the ith segment.

The equipment needed includes the sample Sa1, the emitter, the target, two electrometers for measuring charges, the filament supply, and the acceleration supply.

Firstly, we check all the electrical connections, calibrate the strip-chart recorder, and connect two segments to the electrometers while other segments are grounded. Then we raise the filament voltage to produce the desired beam current. The charge measurements proceed as follows:

a) Raise acceleration voltage to the desired value. Wait for a few seconds to charge the sample, but not so long that the accumulating electrons on the surface drift through the thin film.

b) Register the maximal charge readings on both M1 and M2.

c) Discharge the sample by decreasing the acceleration voltage to zero gradually. This step should be done slowly. Otherwise, there would be residual charges on the sample.

d) Register the readings on both electrometers when acceleration voltage is zero.

e) The accumulated charge for the segment connected to M1 under that beam voltage is the algebraic subtraction of the second reading (in d)) from the first reading (in b)) on M1. The charge on the segment connected to M2 is a similar subtraction of readings on M2. We may repeat this procedure a) - e) two or three times to be sure of the charge value obtained. Generally, it is nearly constant in the measurements for each segment. If not, we take the

average value. Charges for other segments are found by connecting the electrometers to corresponding positions in Fel and by repeating the procedure a) - e).

Capacitances are measured directly for each segment by placing a drop of aqueous salt solution, which acts as an electrode, on the dielectric surface and applying potentials of 500 V and 1,000 V across the film. Corresponding charges q_1 and q_2 are read on one electrometer. Usually, the capacitance for a particular segment is taken to be $q_1/500$ which is the same as $q_2/1,000$. Capacitance measurements are done outside the vacuum.

3. Method Number 2

The objective of this method is to measure secondary-electron emissions from a sample, which has been already charged up with a charging beam, when it is irradiated by a probing beam acting as the primary beam. The approach is an effort to distinguish the two types of electrons, primary and secondary, via readings of currents which are induced on the sample and the collector.

Sample Sa2 replaces Sa1. In addition to those things used in method 1--the emitter, the target, the electrometers, the filament supply, and the acceleration supply--we need the regulator, the reference supply, the recorder, and for some specific measurements the fine screen which hung above the sample within certain distances from the sample.

As a preliminary, we check all the electrical connections calibrate the recorder and electrometers so that graphs on the recording charge are time varying plots of the electrometer readings. We then connect M2 to the sample Sa2 (one segment only), M1 to the collector and raise the filament voltage to have the wanted beam current density. The secondary electron emission measurements are then made as follows:

a) Open the shutter and the shield so that the sample is entirely exposed through the large hole on the baffle of the regulator.

b) Increase acceleration voltage to the desired value of charging beam voltage. The sample is charged up freely as if the regulator were not there.

c) Wait for a few seconds and then close the shutter and the shield in that order. The charged sample is no longer under the beam's irradiation.

d) Decrease acceleration voltage to probing-beam voltage. This should be done quickly to avoid drifting of the accumulated electrons on the surface through the sample.

e) Set M1 and M2 suitable scales (10^{-9} ampere full scale), and start the recorder. Steps d) and e) should be completed in less than 30 seconds.

f) Open the shutter only, while the shield remains on top of the collector. Hence the unique path for the electrons that strike the sample is a straight line through the tube onto the shield.

g) Simultaneously with f), let the recorder draw instantaneous responses of the meters due to the induced currents on the sample (M2) and on the collector (M1). We repeat the procedure a) - g) with the probing beam voltage varying from a small level, say the primary voltage less 2,000 volt, to the charging beam voltage in steps of 50.0 volt measured against the reference voltage.

Results from method 1 show us that the sample's surface voltage, namely the threshold voltage, is within 3,000 volt of the primary beam voltage. Method 2 is based on the assumption that we have a reading on M2 (sample) whenever the secondary beam voltage is greater than the threshold voltage. Otherwise, the beam will be reflected by the negative surface potential and collected by the collector.

We must accelerate the beam with two different levels in two unlike environments. The higher level beam, the charging beam, charges the sample up openly. The lower level beam, the probing (primary) beam, irradiates the charged sample with the narrowed beam passing through the tube. The tube is oriented to the center of the sample and it is small enough so that the spreading electrons do not strike the aperture or the collector. Therefore, as soon as they enter the tube, the primary electrons (probing beam electrons) must be in one of the two following instances: 1) They are reflected and collected if the probing beam voltage is smaller than the threshold voltage. There is no response on

electrometer M2 and a constant induced current on electrometer M1. 2) They strike the sample if the probing beam voltage is greater than or equal to the threshold voltage. Then secondary electrons are given off from the sample. Consequently, the responses occur on both electrometers, and therefore, two graphs versus time appear on the recording chart. The graph corresponding to the collector is the voltage induced by the emitted-secondary electrons. The graph corresponding to the sample is the induced voltage due to the secondary electrons minus primary electrons entering through the tube. Information contained in the graphs shall be further analyzed in Chapter IV, Section A.

4. Time constant measurement

For calculation in Chapter IV, one needs to know the time constant of the circuit from the sample through the electrometer M2 to the graph on the recording chart. It is measurable by method 2 with the primary (probing) beam irradiating the sample for a short duration t_s (fraction of a second). The induced current $i_2(t)$ on the sample becomes a pulse. The graph becomes a pulse response of the low-pass filter as shown in Fig. (II-6). On the graph we select one point $(t_r, v(t_r))$ to be the reference. The time constant is the difference t minus t_r with t satisfying $v(t) = v(t_r)/e^{-1}$. The time constant is measured in the same environment where the secondary electron

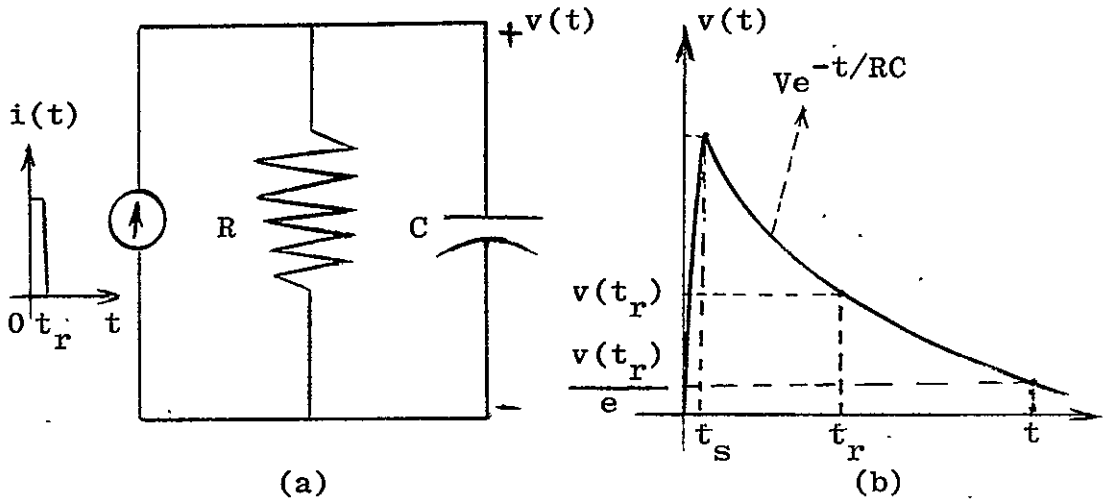

Figure (II-6) a. A low pass filter with a pulse input
b. One way to measure the time constant from the response: $RC=t-t_r$ for $t_r>t_s$.

emission happens. It varies from case to case, with the screen or without the screen and somewhat with the amount of charge accumulated on the sample's surface.

III. FIELD MAPPING ABOVE A DIELECTRIC SURFACE

After a few measurements with sample under circular apertures having radii of 2.5, 3.8 and 5.1 cm, the fact became apparent that the voltage gradient is unchanged near the edge as shown in Fig. (III-1b). This leads us to the proposition that effects of walls other than those at A and C do not appear in the variation of potential along x-direction, and that along z-direction illustrated in Fig. (III-1a) the potential can be regarded as a constant. In other words, the surface's potential changes with x only.

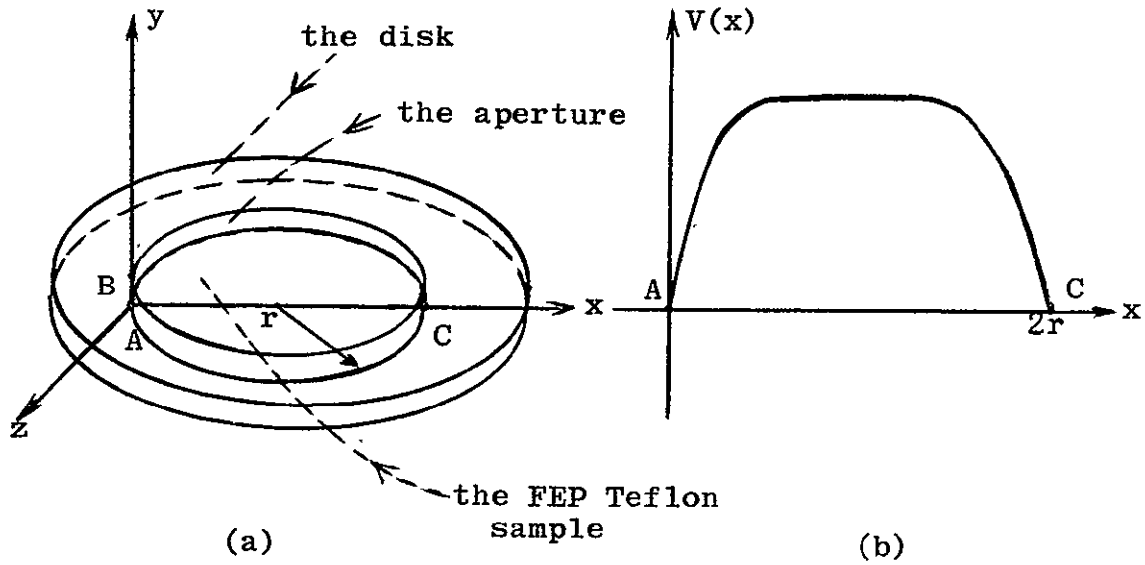

Figure (III-1) a. The three-dimensional specimen
b. An ordinary shape of voltage rapidly decays near the edges. For three different apertures, flat interval is longer for a larger radius sample.

A. Analytic Considerations

In many practical situations, the boundary, either itself or after some complex transformations, is a plane with a potential specified as a function of only one variable. Therefore, the region of interest which is the upper half space limited by the plane reduces a two-dimensional boundary value problem. The solution with Dirichlet boundary conditions [17], which is proved in Appendix A1.1, for an arbitrary position vector $\vec{v}$ becomes

$$\phi(\vec{v}) = \frac{-1}{4\pi} \int_{S'} \phi(\vec{v}') \quad \frac{\partial G}{\partial n'} \ (\vec{v};\vec{v}')ds'$$

where $G(\vec{v};\vec{v}')$ is a Green's function and the prime refers to the boundary.

Suppose the boundary potential is given by

$$\phi(\vec{v}') = V(x') \ , \qquad y' = 0 \ .$$

Accordingly, the potential for $y \geq 0$ is z-independent as shown in Figure (III-2a). The Green's function is the potential at $\vec{v} = (x,y)$ due to a unit line charge at $\vec{v}' = (x',y')$, while the x-z plane is grounded as illustrated in Figure (III-2b). Via the method of images, the total potential for $y>0$ is found to be

$$G(\vec{v};\vec{v}') = - \ell n \ \frac{(x-x')^2+(y-y')^2}{(x-x')^2+(y+y')^2} \ ,$$

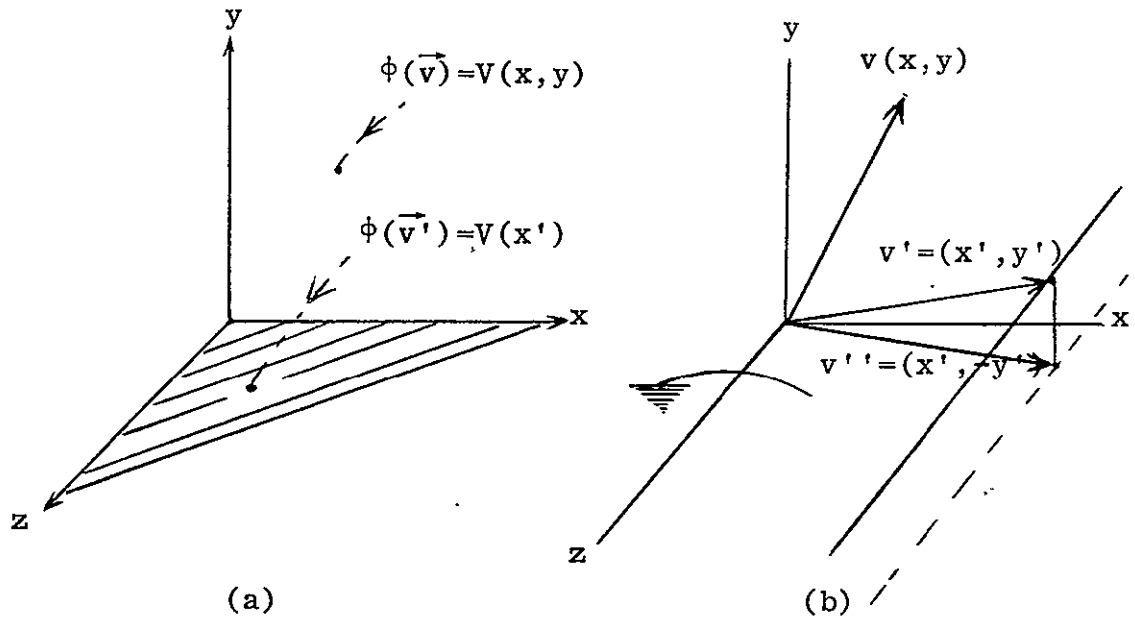

Figure (III-2) a. Dirichlet boundary conditions
b. Method of images

so that on the plane $\vec{v'} = \vec{v''} = (x',0)$, $G(\vec{v};\vec{v'}) = 0$ the boundary condition is satisfied [18]. Subsequently, the normal derivative on S' is

$$\left.\frac{\partial}{\partial n'}G(\vec{v};\vec{v'})\right|_{(S')} = \left.\frac{\partial}{\partial y'}G(x,y;x',y')\right|_{y'=0}$$

$$= \frac{-4y}{(x-x')^2+y^2} .$$

The final formulation of a potential at a point (x,y), y>0, is achieved:

$$P(x,y) = \frac{1}{\pi}\int_{-\infty}^{\infty} \frac{V(x')y}{(x-x')^2+y^2}\,dx' \qquad \text{(III-1)}$$

The electric field is then derived from the potential:

$$E(x,y) = \frac{1}{\pi}\int_{-\infty}^{\infty} \frac{V(x')\,dx'}{[(x-x')^2+y^2]^2} \cdot$$

$$\cdot\left\{2(x-x')y\hat{\epsilon}_x + [y^2-(x-x')^2]\hat{\epsilon}_y\right\} \qquad \text{(III-2)}$$

where $\hat{\epsilon}_x$ and $\hat{\epsilon}_y$ are unit vectors.

Let the voltage distribution on the boundary be piecewise linear, as shown in Figure (III-3). Then the

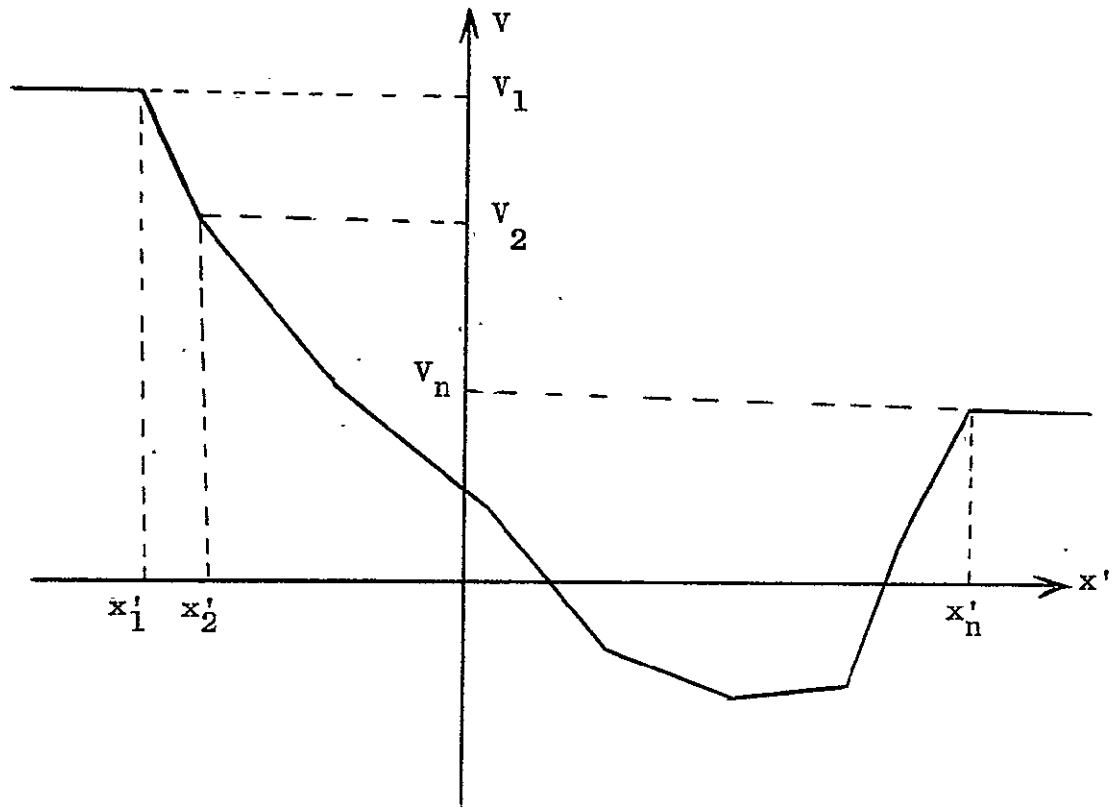

$$V = \beta_i x' + \alpha_i \text{ for } x'_i \leq x' \leq x'_{i+1}$$

Figure (III-3) Piecewise linear voltage distribution for n points with constant wings. V_1 and V_n may be negative, zero, or positive.

linear functions of V(x') are substituted into the expressions for P(x,y) and E(x,y) to yield the following:

$$P(x,y) = \frac{1}{2}(V_1+V_n) + (V_1T_1-V_nT_n) + \sum_{i=1}^{n-1}[(\beta_i x+\alpha_i)(T_{i+1}-T_i)+\beta_i y(L_{i+1}-L_i)] \qquad \text{(III-3)}$$

$$E_x(x,y) = (V_1G_1-V_nG_n) + \sum_{i=1}^{n-1}[(\beta_i x+\alpha_i)(G_{i+1}-G_i) + \beta_i y(F_{i+1}-F_i)-\beta_i(T_{i+1}-T_i)]$$

$$E_y(x,y) = (V_1F_1-V_nF_n) + \sum_{i=1}^{n-1}[(\beta_i x+\alpha_i)(F_{i+1}-F_i) - \beta_i y(G_{i+1}-G_i)-\beta_i(L_{i+1}-L_i)] \qquad \text{(III-4)}$$

where

$$D_i = \frac{1}{\pi[(x_i'-x)^2+y^2]}$$

$$F_i = (x_i'-x)D_i$$

$$G_i = y\ D_i$$

$$T_i = \frac{1}{\pi} \arctan\left(\frac{x_i'-x}{y}\right)$$

$$L_i = \frac{1}{2\pi} \ell n[y^2+(x_i'-x)^2] \quad .$$

B. Discrete Numerical Approach

Having established compact forms for $P(x,y)$, $E_x(x,y)$, and $E_y(x,y)$ enables us to compute coordinates of points on a characterized equipotential contour and electric field which is normal to the contour at each point. For a given $P(x,y) = P$ in the interval $[V_i, V_{i+1}]$, we can always identify a point $(x_o,0)$ on the x-axis where

$$x_o = \frac{P-\alpha_i}{\beta_i} \quad . \qquad \text{(III-5)}$$

Since Equations (III-3) and (III-4) do not hold when $y=0$, the subsequent point is assigned a small y value and has coordinates as follows:

$$x_1 = x_o \ ,$$

$$y_1 = \frac{x_{i+1}'-x_i'}{200} \quad . \qquad \text{(III-6)}$$

One calculates the field at this point and then traces along it, as illustrated in Figure (III-4), to obtain

$$x_1(\text{new}) = x_1 + D\,\frac{E_x}{E_x^2+E_y^2}$$

$$y_1(\text{new}) = y_1 + D\,\frac{E_y}{E_x^2+E_y^2} \qquad \text{(III-7)}$$

where $D = P(x_1,y_1)-P$ controls the size of the step.

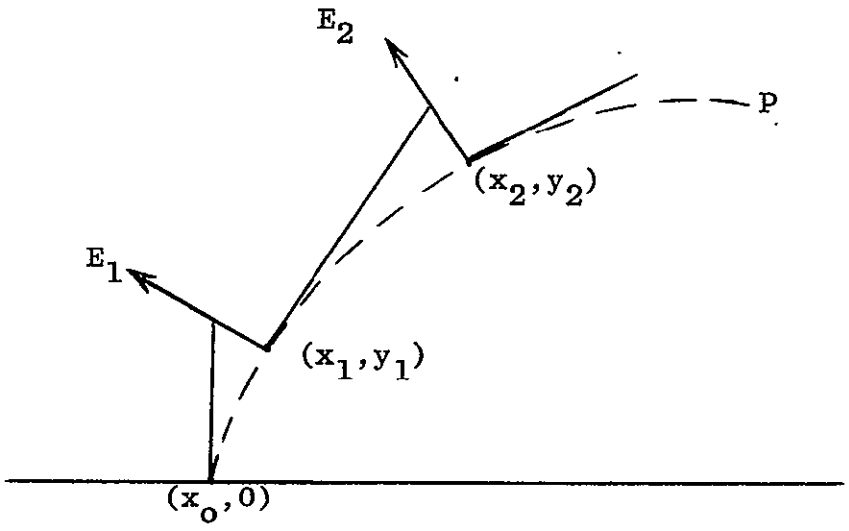

Figure (III-4) A combination of steps, perpendicular and parallel to the field, that converge to a new point on the P contour (shown dashed).

The new pair (x_1,y_1) is substituted into Eqn. (III-2) to check whether the difference between P and $P(x_1,y_1)$ is less than some criterion of convergence of not, i.e.,

$$\left|P(x_1,y_1)-P\right| \leq \frac{|\text{PSTEP}|}{10^4} \qquad \text{(III-8)}$$

where PSTEP is some constant depending upon the range of P. Steps parallel to the field are repeated as necessary.

The next point is found by making a step perpendicular to the field to obtain

$$x_2 = x_1 - A|\text{PSTEP}| \frac{E_y}{E_x^2+E_y^2}$$
$$y_2 = y_1 + A|\text{PSTEP}| \frac{E_x}{E_x^2+E_y^2} \qquad \text{(III-9)}$$

where $-1 \leq A \leq 1$ is used to select the size of the step; its sign is opposite to that of β_i. Field $\vec{E}(x_2,y_2)$ is then computed and Eqn. (III-7) is applied iteratively until the criterion, Eqn. (III-8), is satisfied. This process is repeated over and over until we gain the desired number of points or until we enter a region where E is very small.

C. Experimental Results

1. A sample under a circular aperture

For a 13 mm radius sample of FEP Teflon with a 20 kV electron beam, the voltage distribution measured on the sample's surface is given by Table (III-1) where u is the distance from the left edge. The geometry shown in Figure (III-5) can be converted to a plane with only one conformal mapping if the right hand edge is assumed to be at infinity. Letting $z = z+iy$ and $w = u+jv$, one finds that the appropriate transformation [19] is

$$w = \frac{1}{\pi}\,[s+\ell n(s+z)], \qquad s = \sqrt{z^2-1} \quad . \qquad \text{(III-10)}$$

Also, Eqn. (III-10) is employed with real z and w to find the points on the z-plane (y=0) corresponding to the data shown in Table (III-1).

A brief review of Eqn. (III-3) and (III-4) suggests that we linearly interpolate the data, and that the set of coefficients is given by

$$\beta_i = \frac{V_{i+1}-V_i}{x_{i+1}-x_i}\,, \quad \alpha_i = V_i-\beta_i x_i,$$

$$i = 1,\ldots,n-1 \quad . \qquad \text{(III-11)}$$

The two wings are given as

$$V = V_1 = 0 \qquad \text{for} \qquad x \leq x_1 = 1.0$$

$$V = V_n = -17.0 \qquad \text{for} \qquad x \geq x_n = 27.43 \quad .$$

The method described in Section B was carried out to find the contours from -2 to -16 kV in steps of -2 kV. The data points describing the contours were converted back to the original w-plane via Eqn. (III-10).

For the field components, the formalism of conversion is somewhat different. Since they are analytic functions of (x,y) we invoke Cauchy-Riemann conditions to relate field components E_u, V_v on the original plane to the field

Table (III-1) Data points representing surface potential

Potential (kV)	Coordinate	Transformed Coordinate
0.0	0.0	1.00
-1.5	0.1	1.01
-3.0	0.2	1.05
-4.5	0.3	1.11
-6.0	0.4	1.19
-7.5	0.5	1.29
-12.8	2.0	4.27
-15.0	3.7	8.81
-16.0	5.5	13.99
-16.5	7.0	18.41
-17.0	10.0	27.43

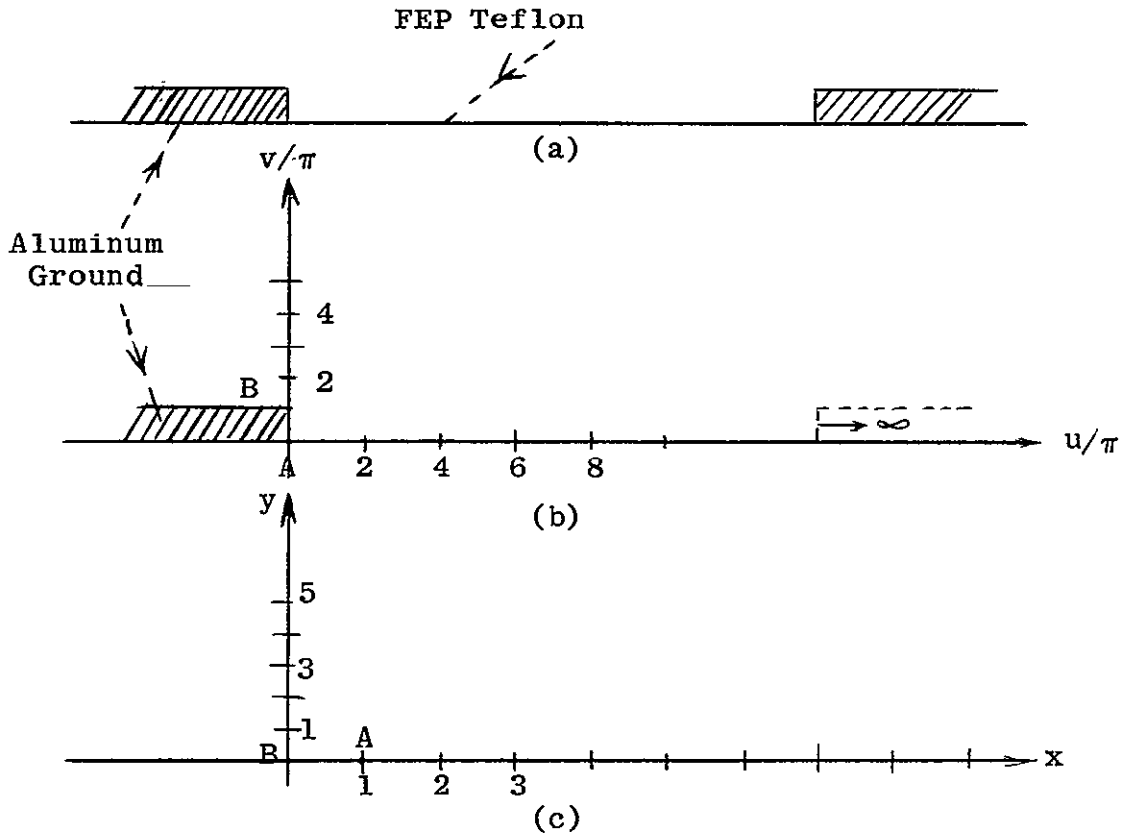

Figure (III-5) a. the actual specimen
b. the approximated specimen
c. the conformed geometry

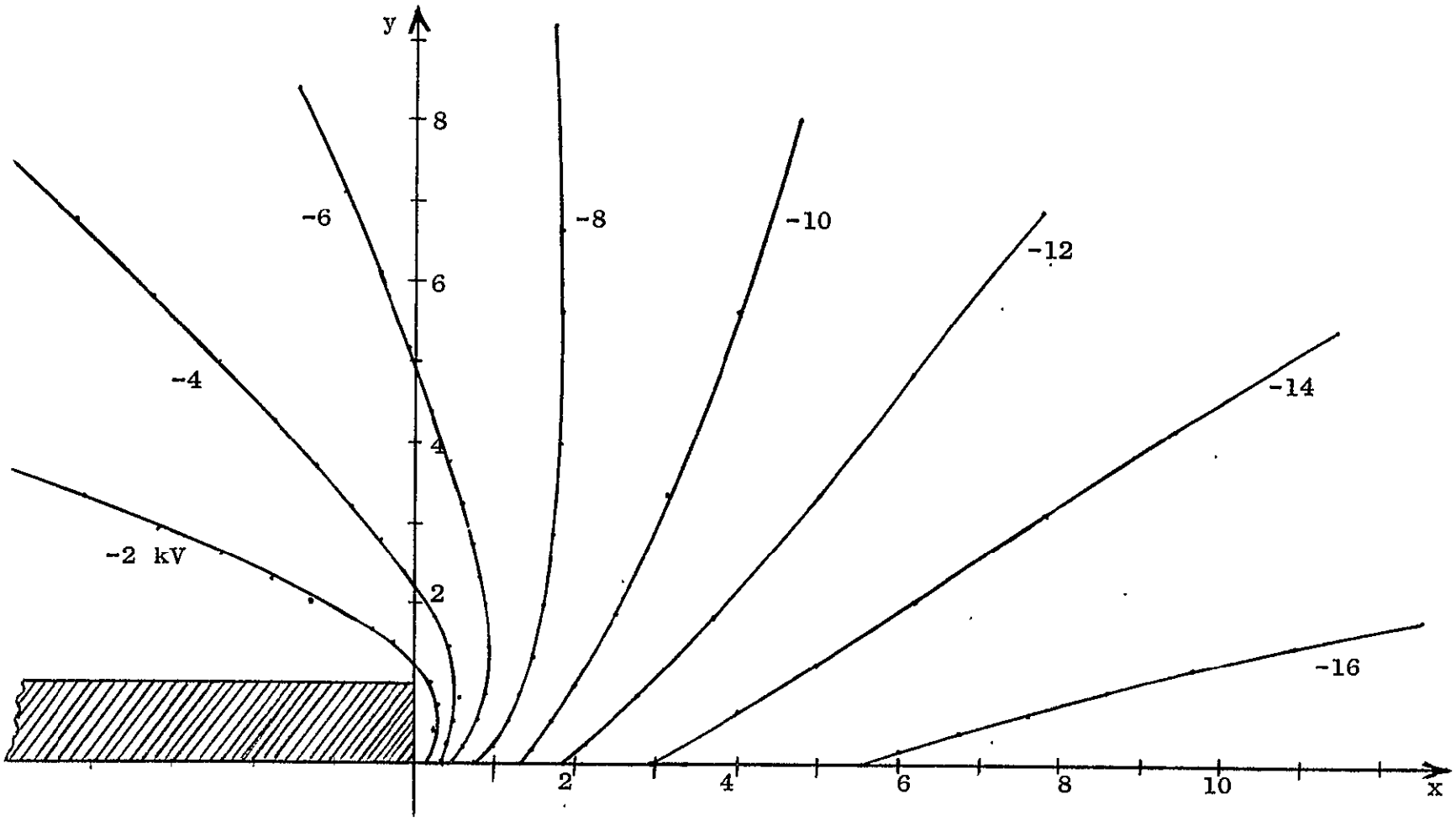

Figure (III-6) Equipotential contours near a charged FEP Teflon surface in a 20 kV beam.

components E_x, E_y on the transformed plane. It is shown in Appendix A1.2 that

$$E_u = \frac{1}{2}[E_x \, Re\{f'\} + E_y Im\{f'\}]$$

$$E_y = \frac{1}{2}[-E_x Im\{f'\} + E_y Re\{f'\}] \qquad \text{(III-12)}$$

where

$$f' = \frac{dz}{dw} = \pi\left(\frac{s}{z+1}\right)$$

is obtained from Eqn. (III-10). This sequence of Eqns. (III-1) to (III-12) and Table (III-1) were implemented with a computer as illustrated in Appendix A3. The outputs are plotted in Fig. (III-6).

2. Sample under two rectangular apertures separated by a hemicylinder

Similarly to the sample under a circular aperture, we first extend the outer boundaries to infinity, as shown in Fig. (III-7) (providing that the hemicylinder's radius is small compared to the sample dimensions) and then straighten the hemicylinder out via the transformation [19]

$$z = w + \frac{1}{w} \quad . \qquad \text{(III-13)}$$

For the field components, we use

$$f' = 1 - \frac{1}{w^2} \quad . \qquad \text{(III-14)}$$

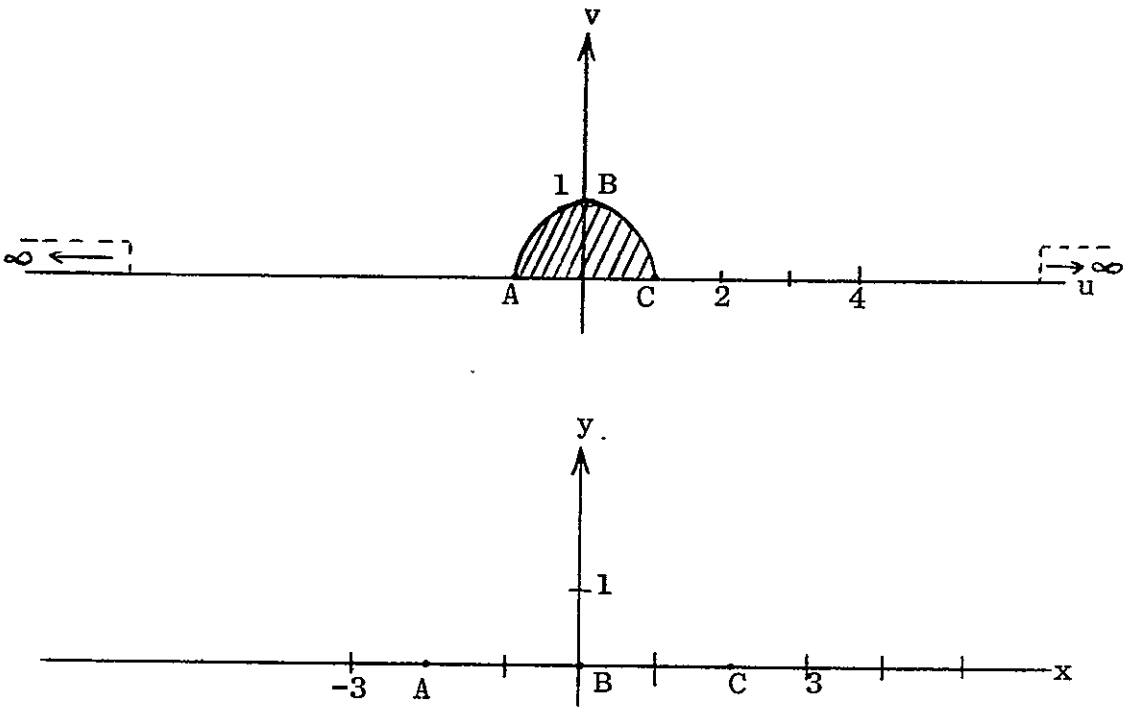

Figure (III-7) Transformation of the system with a hemicylindrical ground strip.

Again, the sequence of Eqns. (III-1) to (III-12), where (III-13) and (III-14) take the place of (III-10) and (III-12), respectively, were carried out to find the equipotentials and field. Table (III-2) displays the data used for this example and Fig. (III-8) shows a plot of the outputs.

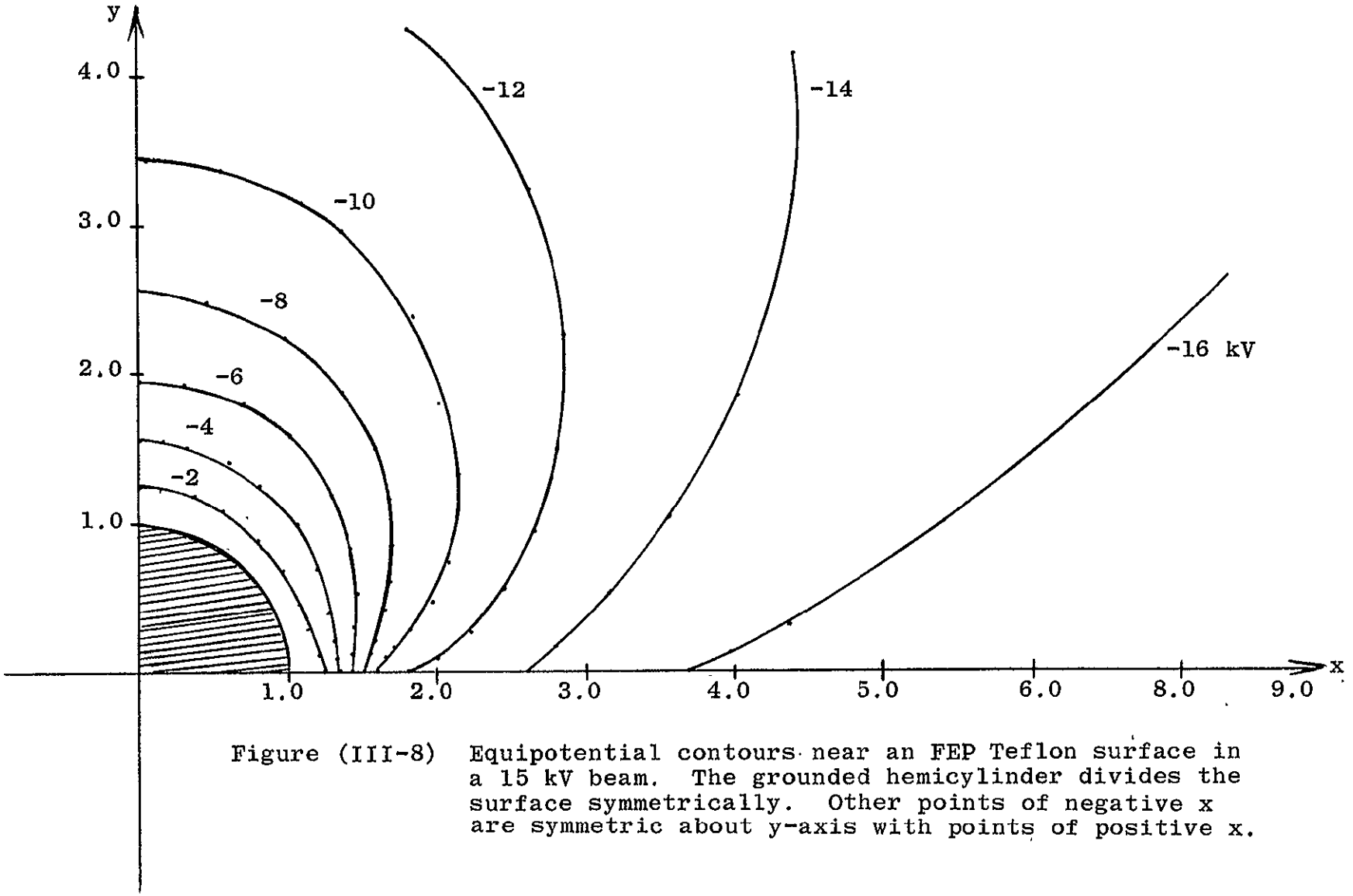

Figure (III-8) Equipotential contours near an FEP Teflon surface in a 15 kV beam. The grounded hemicylinder divides the surface symmetrically. Other points of negative x are symmetric about y-axis with points of positive x.

Table (III-2) Data points representing surface potential. The specimen is symmetric and so is the voltage on its surface.

Potential (kV)	Coordinate	Transformed Coordinate
-17.4	-7.144	-7.284
-17.2	-5.661	-5.837
-16.1	-3.754	-4.021
-14.8	-2.907	-3.2511
-11.6	-1.636	-2.247
0.0	-1.000	-2.000
0.0	1.000	2.000
-11.6	1.636	2.247
-14.8	2.907	3.251
-16.1	3.754	5.837
-17.2	5.661	7.284
-17.4	7.144	

IV. INFLUENCE OF FIELD UPON SECONDARY ELECTRON EMISSION

In the preceeding chapter, we portrayed equipotentials and fields calculated from the voltage distribution on the sample's surface which had been measured via method 1. In this chapter, we shall calculate secondary electron emission coefficients for which data were taken via method 2. The interpretation involves solving an inhomogeneous differential equation where the right-hand side is the sample's substrate current source. The topic of secondary electron emission with field is examined in the last section.

A. Analysis

Based on the continuity relationship between current and charge, the following arguments deal with currents (or voltages) induced by charge (electron) fluctuations. What we could see are outputs of two parallel RC filters on a recording chart as illustrated in Fig. (IV-1). There are always two curves $v_1(t)$ and $v_2(t)$ associated with each measurement.

The response $v_1(t)$ of the R_1C_1 circuit is produced by the current $i_1(t)$ flowing from the collector being connected to the electrometer M1. When secondary electron emission reaches its steady state, the number of primary electrons striking the sample equals the number of secondary electrons released from the sample. The current $i_1(t)$ becomes a constant I_1, and then $v_1(t) = R_1I_1$ is the voltage created by primary electrons. The response $v_2(t)$ of the

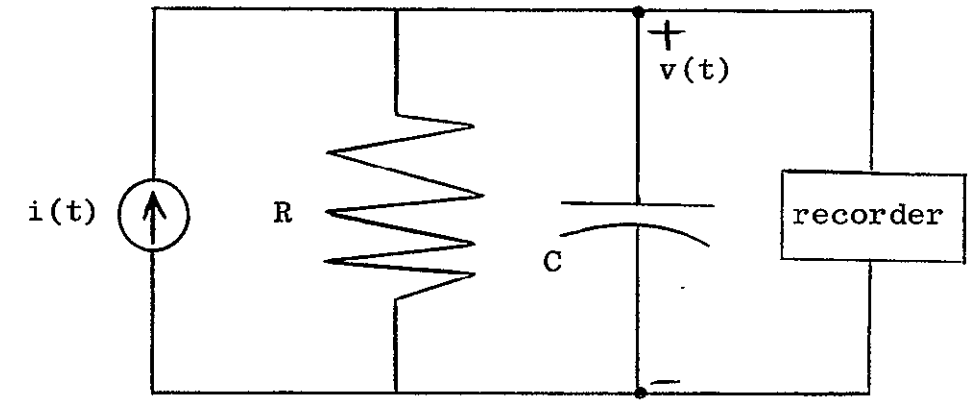

(a)

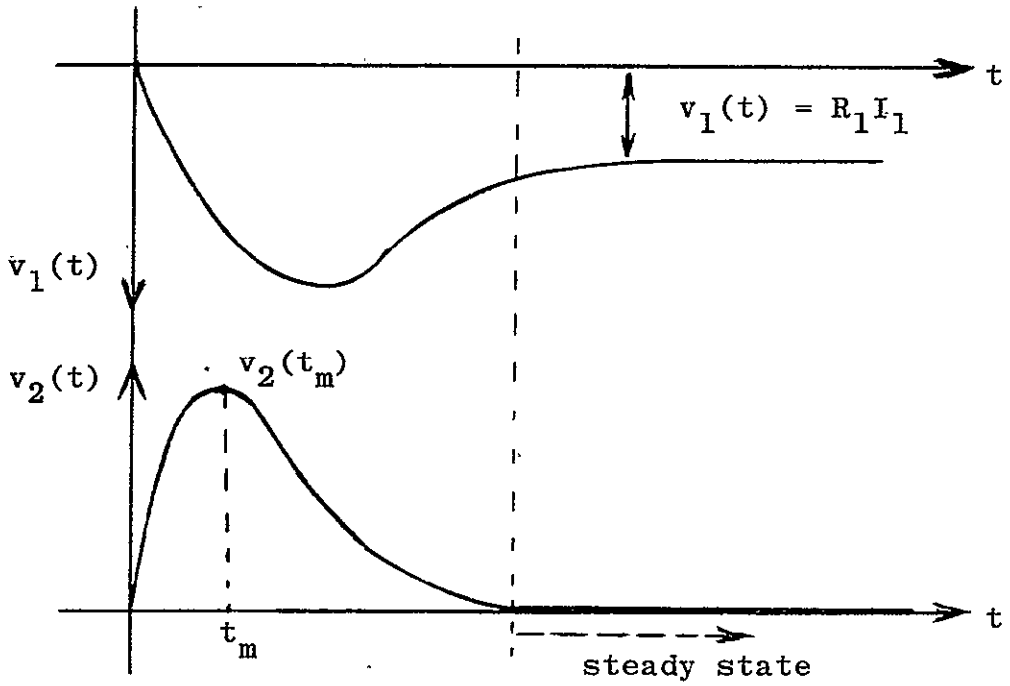

(b)

Figure (IV-1) a. Schematic of recording circuit.

b. Typical outputs of two RC circuits on the chart.

R_2C_2 circuit due to the current $i_2(t)$ is induced by the number of electrons disappearing from the sample surface, secondary electrons less primary electrons. It is the solution of the first order differential equation

$$1/R_2\ v_2(t) + C_2\ dv_2(t)/dt = i_2(t) \quad .$$

After several attempts, we arrived at a physically reasonable assumption for $i_2(t)$, that is $i_2(t) = I_2e^{-t/\tau}$, $t \geq 0$. In a sense, the emission from the surface is greatest at the instance $t = 0$ when we first irradiate the surface which was already charged. There are two unknowns, I_2 and τ with I_2 representing the maximum difference between numbers of electrons arriving and leaving at the sample's surface. We solve the differential equation with the condition that there is no stored energy initially in the capacitor, $v_2(o) = 0$. The solution has the form

$$v_2(t) = \frac{I_2R_2\tau}{(R_2C_2-\tau)} \left[e^{-t/R_2C_2} - e^{-t/\tau} \right], \qquad \text{(IV-1)}$$

where R_2C_2 is measurable and varies with cases.

Even though the forcing function is strongest at $t = 0$, the response is maximum at $t_m > 0$ due to a delay of the R_2C_2 filter, i.e.,

$$\left.\frac{d}{dt} v_2(t)\right|_{t_m} = \frac{I_2 R_2 \tau}{(R_2 C_2 - \tau)} \left[\frac{-e^{-t/R_2C_2}}{R_2C_2} + \frac{e^{-t/\tau}}{\tau} \right]$$

$$= 0 \quad , \qquad \text{(IV-2)}$$

where t_m and $v_2(t_m)$ are read from the chart. Substituting tm into Eq. (IV-2), we gain the root τ by using a bisection-iterative method. Using τ, t_m, and $v_2(t_m)$, we compute R_2I_2 from Eq. (IV-1). With R_1I_1 explained in the foregoing paragraph, the secondary electron-emission coefficient σ is the ratio

$$\sigma = \frac{\text{number of secondary electrons}}{\text{number of primary electrons}} = \frac{I_1+I_2}{I_1} \ .$$

We can choose the scales of both electrometers so that $R_2 = R_1$. Consequently, σ can be written in terms of chart voltages as follows:

$$\sigma = \frac{R_2(I_1+I_2)}{R_1I_1} = 1 + \frac{R_2I_2}{R_1I_1} \quad , \qquad \text{(IV-3)}$$

where R_2I_2 is computed from Eq. (IV-1) and Eq. (IV-2), and R_1I_1 is the steady state voltage due to primary electrons alone read on the plot of $v_1(t)$.

B. Analyzed Data

On each two-graph output shown in Fig. (IV-1), we measure three factors t_m, $v_2(t_m)$ and R_1I_1 to be used in

three equations (IV-1) to (IV-3). The coefficients versus primary beam voltage, Figures (IV-2) to (IV-6), were computed for a 5 mil FEP Teflon sample under a circular aperture having radius of 16 mm with charging beam voltages 10, 15 and 20 kV. The difference between the two beam voltages is E_p.

Looking through Figures (IV-2) to (IV-6) we conceive that the curves are rapidly increasing with primary (probing) beam energies larger than the threshold voltage by a small amount. Within a 200-volt increment, they reach peak values. Then they smoothly decay as the primary beam gets larger. The threshold voltages are always at least 1.2 kV less than the charging beam voltage. If we let the charging beam voltage be the origin, then thresholds of beams of 20.0, 15.0, and 10.0 kV appear in this order with respect to the probing beam. The peak values of the of the coefficient are about two when the screen is low and about 2.8 when the screen is 23 mm high above the sample surface. Note that in all cases, σ is a very sensitive function of secondary beam voltage in the interval around σ_{max}.

C. Accuracy

Looking at Fig. (IV-1) closely, we realize $v_2(t_m)$ can be chosen more precisely than t_m. Since there is a range where we can select a value for t_m, one question arises concerning the sensitivity of σ with respect to the choices of t_m and $v_2(t_m)$, as well with respect to the measured R_2C_2 and the inexactness of the assumed exponential form for $i_2(t)$ in the analysis section.

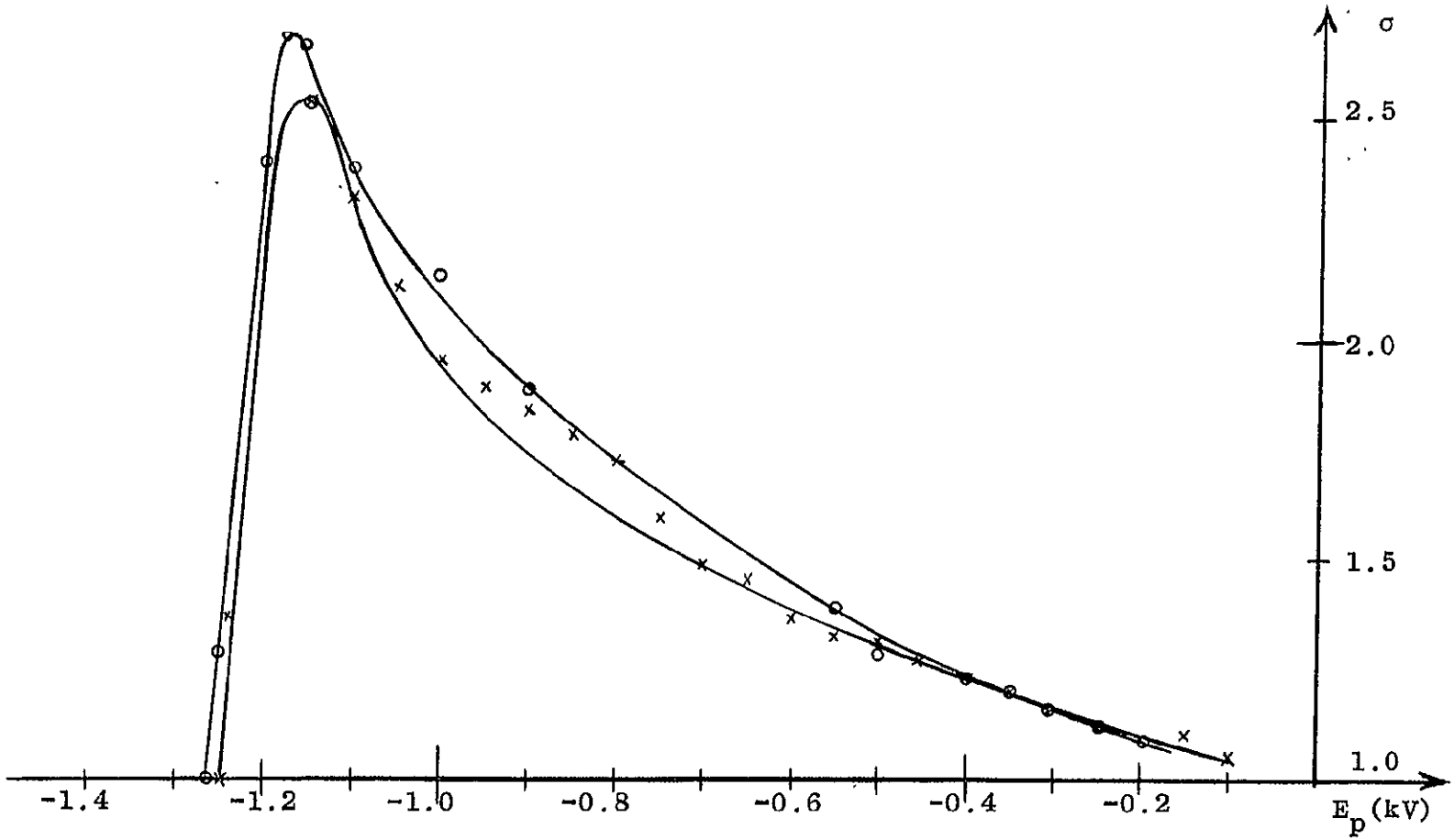

Figure (IV-2) Data for × 10 kV and o 15 kV beams without the screen. The charging beam voltage corresponds to E_p=0.

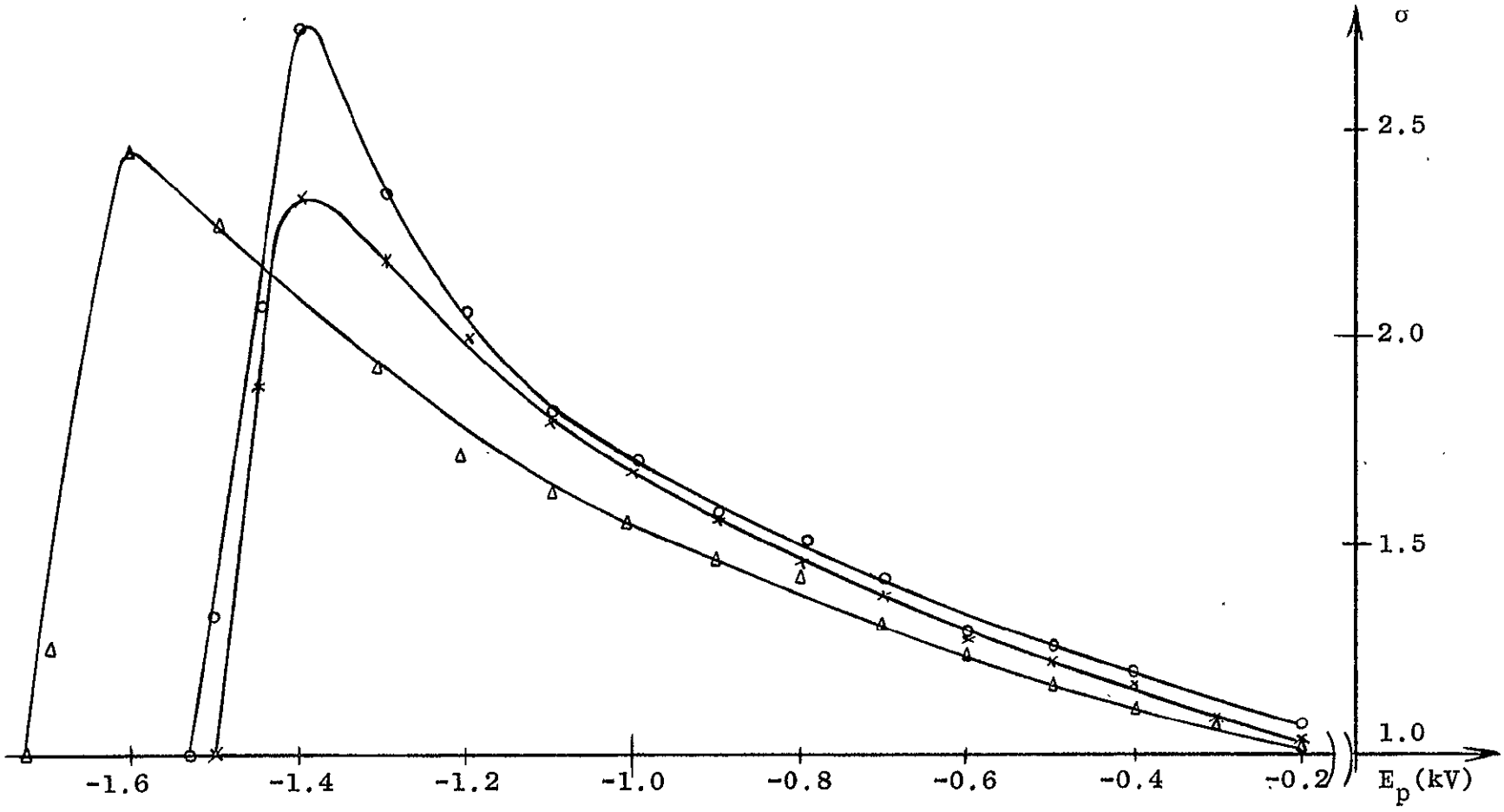

Figure (IV-3) Data for ×10 kV, ○15 kV and △20 kV beams with the screen about 23 mm from the sample's surface.

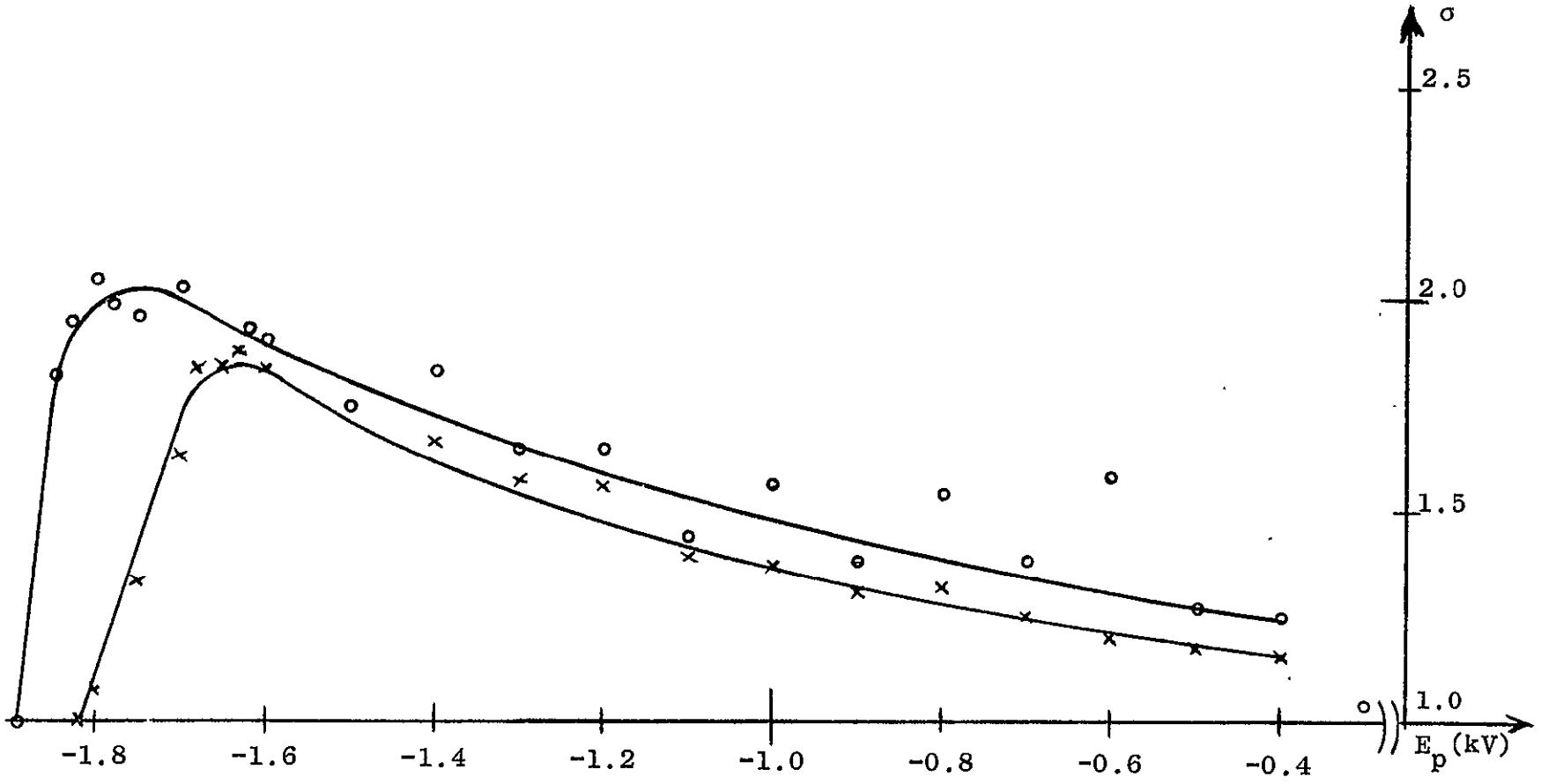

Figure (IV-4) Data for × 10 kV and o 15 kV beams with the screen about 4 mm from the sample's surface.

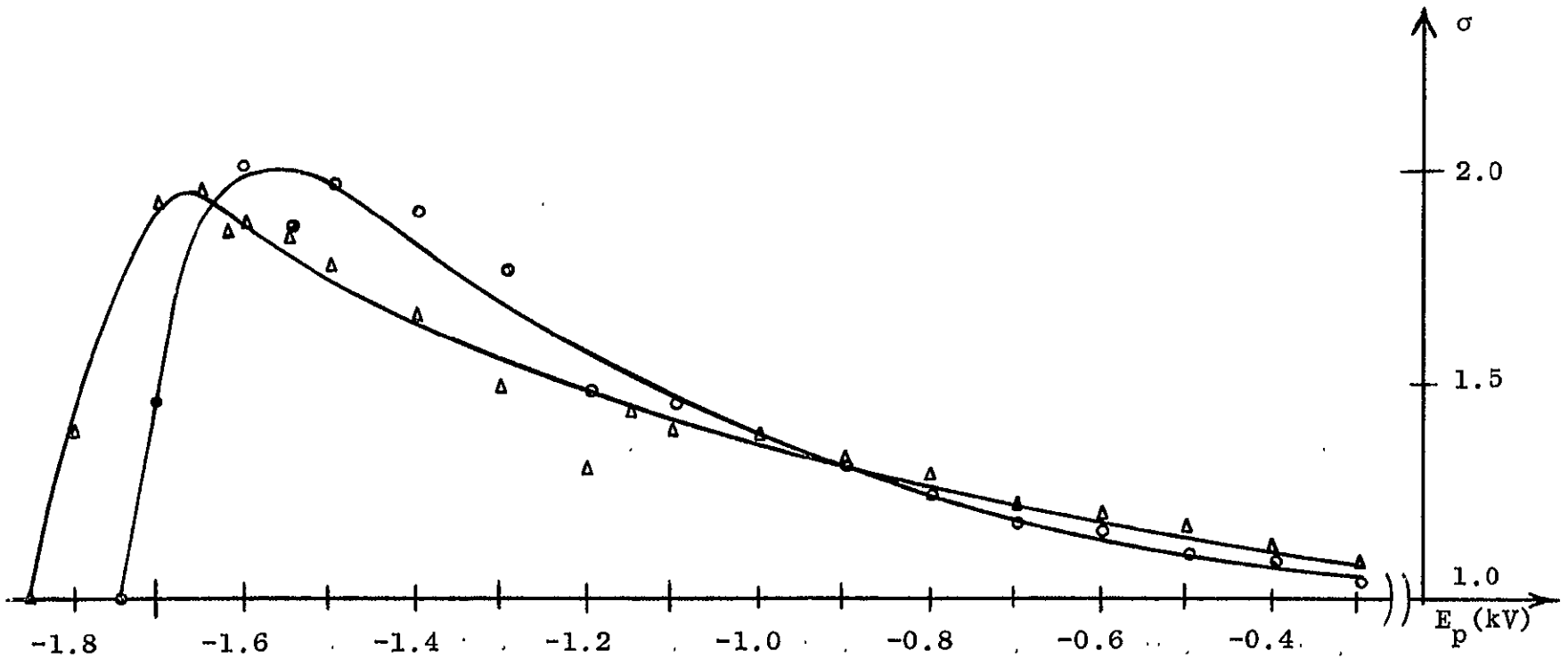

Figure (IV-5) Data for o 15 kV and ∆20 kV beams with the screen about 10 mm from the sample's surface.

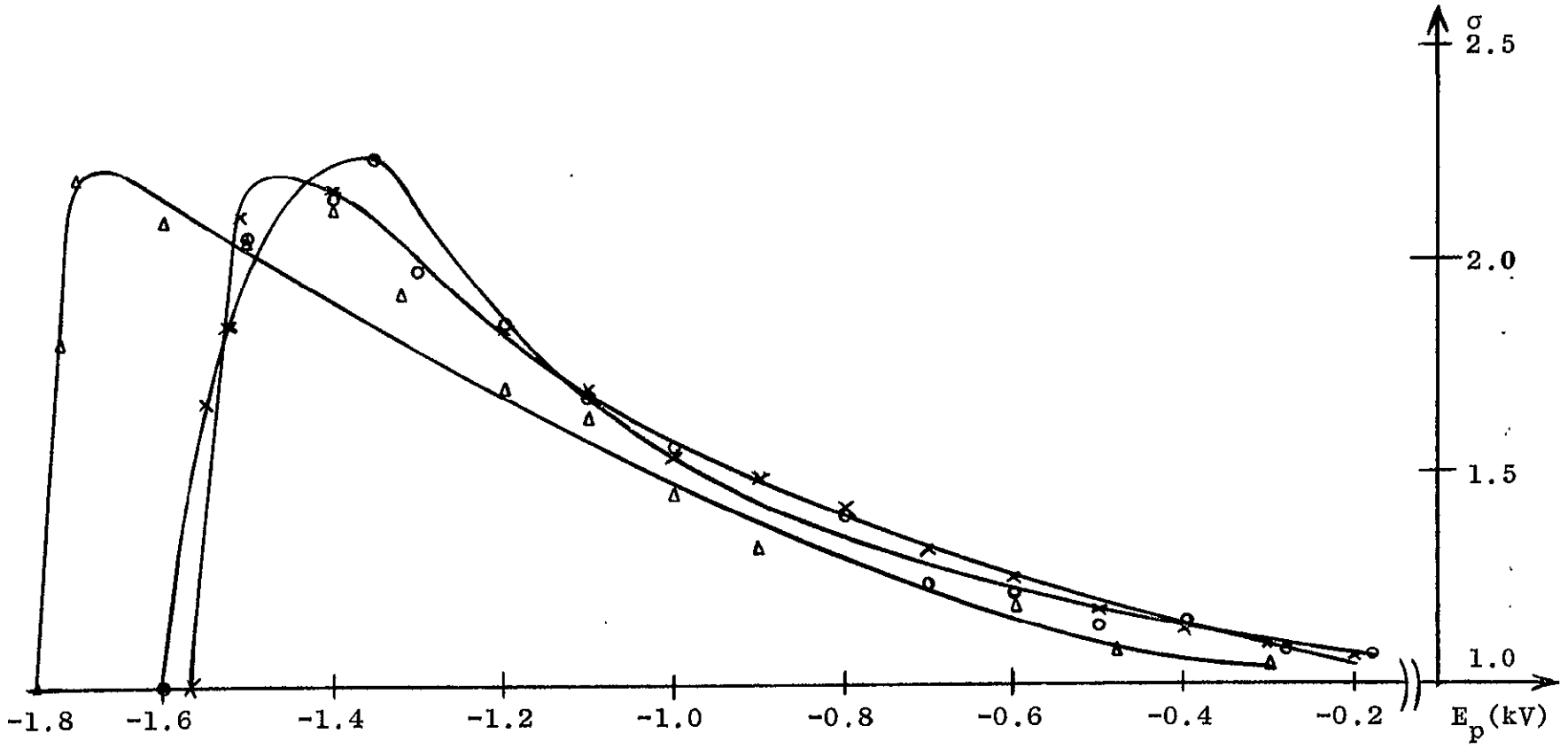

Figure (IV-6) Data for × 10 kV, o 15 kV, Δ 20 kV beams with the screen about 15 mm from the sample's surface.

It was numerically found that

$$\frac{\Delta\sigma}{\sigma} \simeq 0.8 \frac{\Delta t_m}{t_m} \; ; \quad \frac{\Delta\sigma}{\sigma} = \frac{\Delta v_2(t_m)}{v_2(t_m)} \leq 0.02 \; ;$$

$$\frac{\Delta\sigma}{\sigma} \simeq 0.6 \frac{\Delta R_2C_2}{R_2C_2} \; ,$$

where the normal values of t_m and R_2C_2 are respectively

$$t_m = 0.29 \pm 0.025 \text{ sec} \quad \text{and} \quad R_2C_2 = 0.155 \pm 0.01 \text{ sec}^{-1}.$$

Suppose the function $i_2(t)$ produces a 5% error on σ, the largest possible deviation of σ is then

$$\frac{\Delta\sigma}{\sigma} \leq 0.8 \frac{\Delta t_m}{t_m} + 0.02 + 0.6 \frac{\Delta R_2C_2}{R_2C_2} + 0.05 = 0.17768.$$

We would claim that accuracy of this interpretation is within 18%.

D. Field Influence on the Secondary Electron Emission

As a matter of fact, the field had influenced the secondary-electron-emission coefficient computed in Section B. We ought to recognize two kinds of field being present inside the collector where the primary electrons and secondary electrons were captured: The accumulated field is the field due to charge accumulation on the dielectric surface. The enforced field is the field due to the screen's presence.

At the center of the sample toward where the beam was deliberately directed, the field possesses only a y-component because of symmetry of the boundaries. When the screen is near the sample, the enforced field predominates over the accumulated field and the total field is mostly uniform. When the screen is high above the sample, there is a fringing effect on the enforced field and the accumulated field was about equal to the total field. There also exists an electrostatic force which pulls the screen down, i.e., the distance between the screen and the sample is hard to control. Various contributions make it difficult to obtain exact values of the field. Nevertheless, approximations of the field ranges with respect to the screen's position and surface (threshold) voltages tender us an idea of how the characteristics of secondary electron emission vary with field, as illustrated in Table (IV-1) and in Figures (IV-7) to (IV-9).

Fig. (IV-7) shows the differences of the σ curves, with and without the field. As a matter of fact, there are scattered points due to errors made during the measurements and the computation. Scattering is greater when the field is stronger and also the secondary emission peaks are broader. Clearly from Fig. (IV-8), the voltage interval θ between unity crossing points becomes larger with a higher field existing above the surface. When the screen touched the sample, we observed that surface potential could not reach its equilibrium as usual even for a 10 kV beam. The surface

Table (IV-1) Estimated range of $E_y = E_e + E_a$ yielded from the compound of accumulated field E_a (in Chapter III) and the enforced field E_e (surface potential)/(screen's height).

Primary probing beam (kV)	Screen's distance from the sample surface (mm)	Threshold voltage (kV)	Approximated field range E_y (kV/mm)	Note
	4.0 ± 1.0			
	10.0 ± 2.0	18.15	1.82 ± 0.20	
20	15.0 ± 2.0	18.25	1.22 ± 0.25	
	23.0 ± 2.0	18.27	0.80 ± 0.30	
	62.0 ± 0.0			
	4.0 ± 1.0	13.11	3.28 ± 0.15	14.5 kV beam
	10.0 ± 2.0	13.26	1.33 ± 0.20	
15	15.0 ± 2.0	13.40	0.90 ± 0.25	
	23.0 ± 2.0	13.47	0.59 ± 0.30	
	62.0 ± 0.0	13.73	0.22 ± 0.45	without the screen
	4.0 ± 1.0	8.18	2.05 ± 0.15	
	10.0 ± 2.0			
10	15.0 ± 2.0	8.43	0.56 ± 0.20	
	23.0 ± 2.0	8.50	0.37 ± 0.25	
	62.0 ± 0.0	8.75	0.15 ± 0.45	without the screen

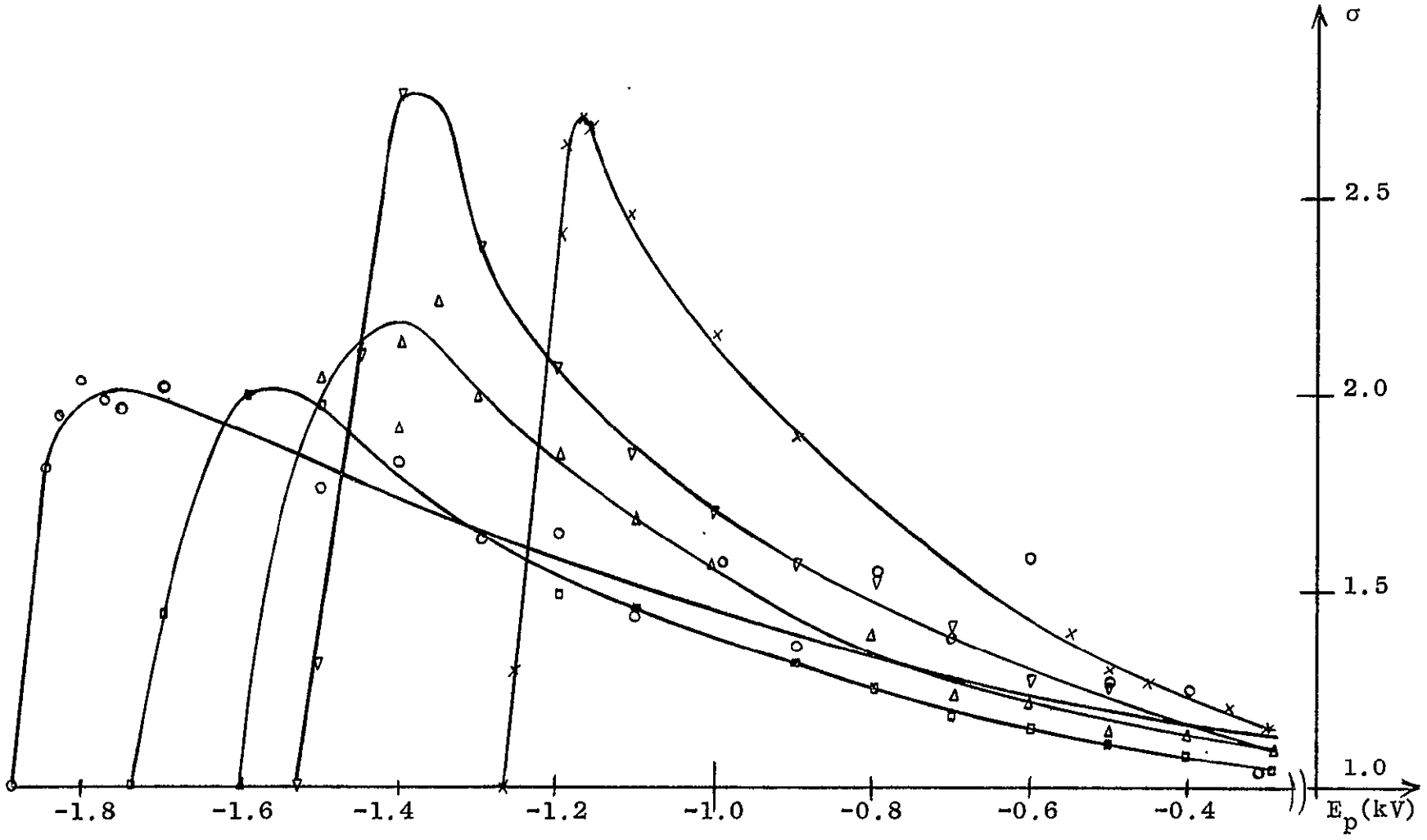

Figure (IV-7) Data for 15 kV beam only with different positions of the screen: × without the screen, ▽ 23 mm, △ 15 mm, ▫ 10 mm, and ○ 4 mm from the sample's surface.

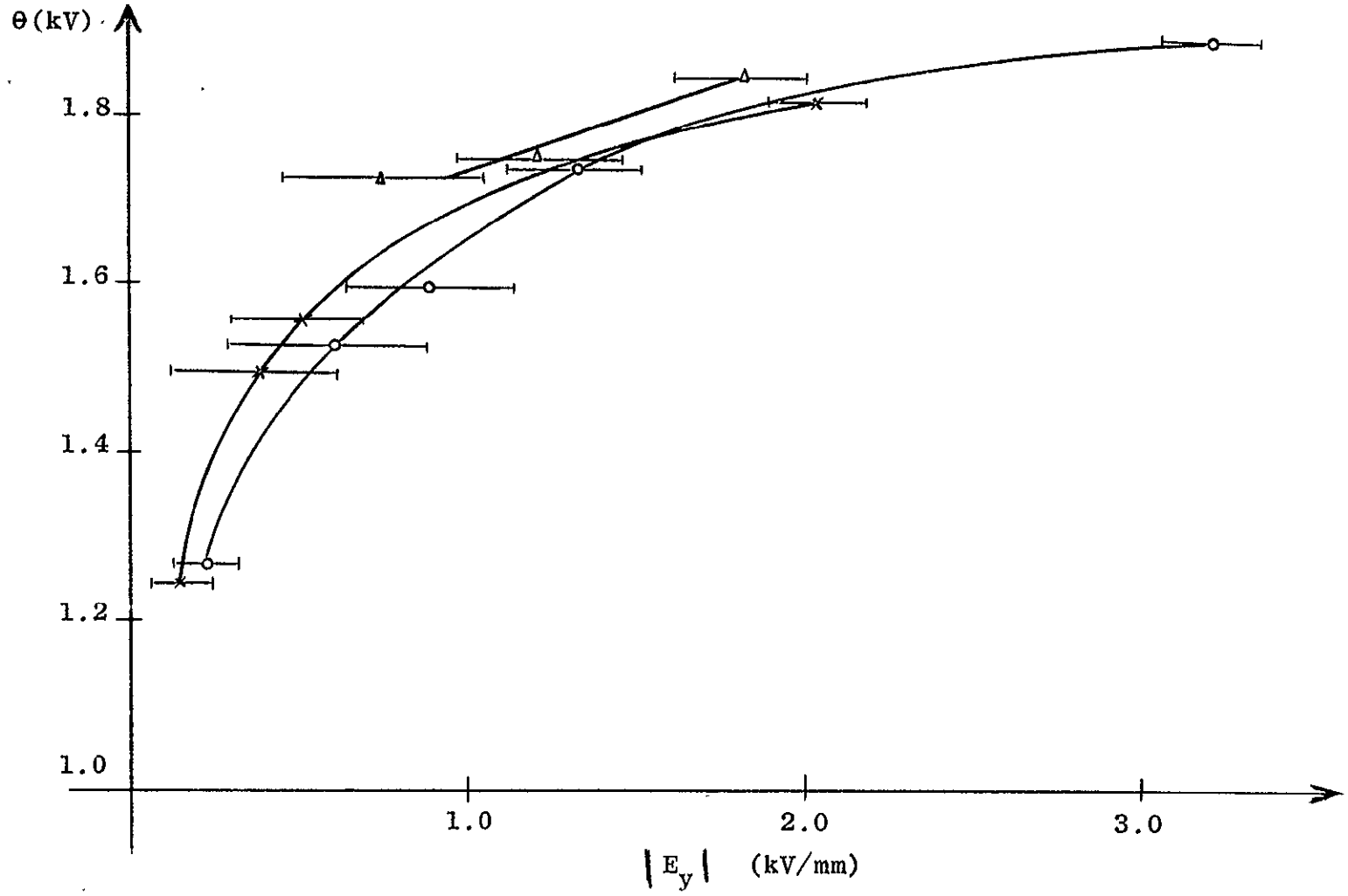

Figure (IV-8) Plots of voltage interval θ versus magnitude of estimated field for × 10, o 15, and ▵ 20 kV beams.

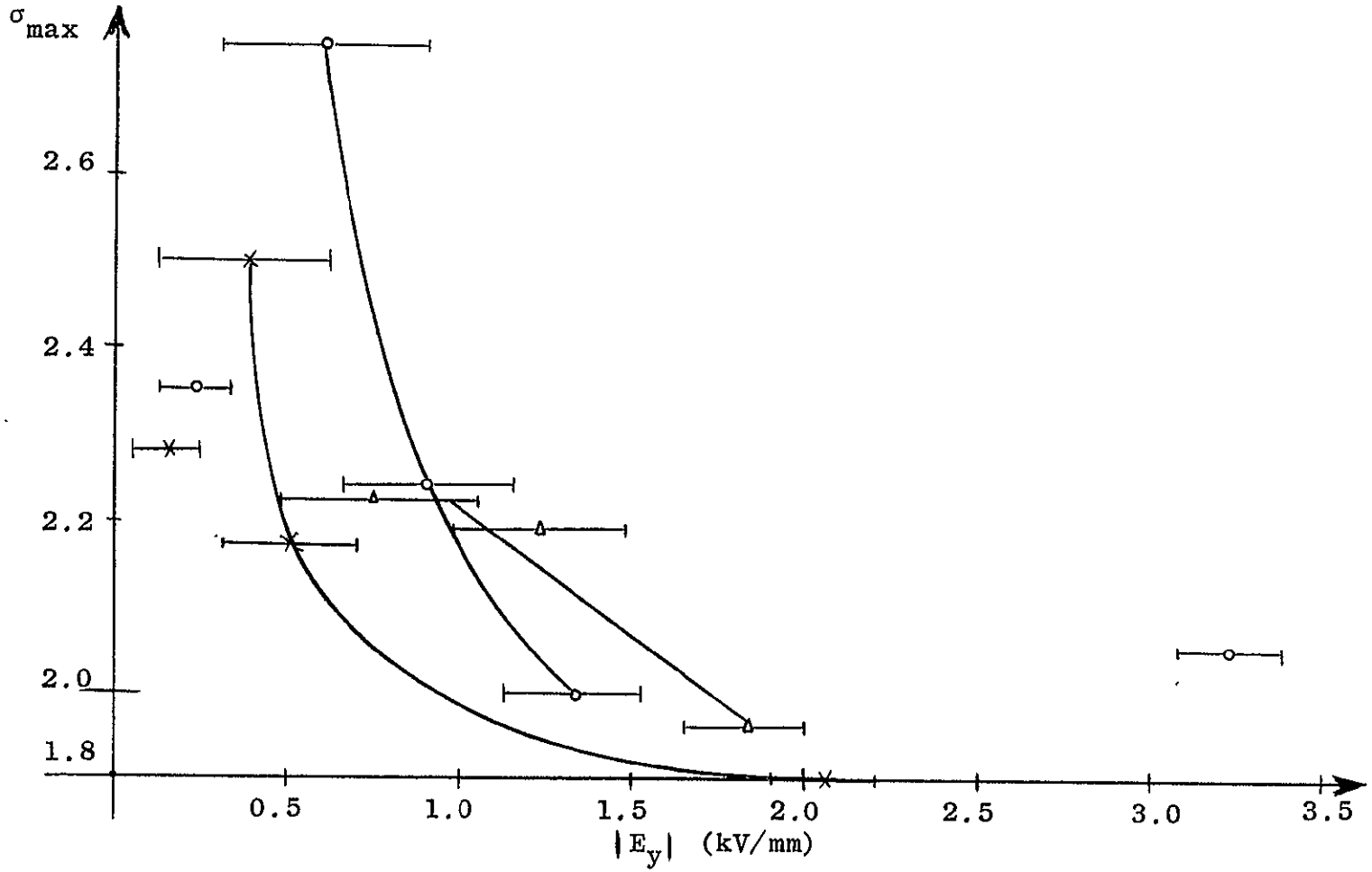

Figure (IV-9) Plots of maximal value of σ versus the magnitude of the estimated field for X 10 kV, o 15, and Δ 20 kV beams.

accumulated charge to some level and then suddenly discharged. Is this due to a very strong field (zero distance of the grounding screen from the charge surface) or an extremely low threshold voltage? We doubt that discharging is caused by secondary electron emission. It is more likely another phenomena which is beyound our scope. For a discussion about discharging (flashover) refer to the report of Robinson [15].

It is logical to think that under the influence of a stronger field the number of secondary electrons liberated from the charged surface by bombardment would be larger. This is, however, not true. Rather, σ_{max} is seemingly a monotonic-decreasing function of field and the sharpness around σ_{max} on the σ-curve is reduced by a high field as shown in Fig. (IV-7) and Fig. (IV-9).

V. SUMMARY AND DISCUSSION

As an analogy, the whole system can be depicted as a two-port network shown in Fig. (V-1), where the "black box" is the vacuum containing a dielectric sample, an electron source, and some apparatus to support the measurements realized outside it. The inputs, filament voltage and acceleration voltage, supply power for the electron gun. The outputs, accumulated charges (or voltages) or induced currents (or voltages), are read on the electrometers or on a recording chart. Inside the vacuum, when the sample is being irradiated by an electron beam, at least two processes take place: charge accumulation on the sample's surface and secondary emission from the sample's surface. They both were qualitatively and quantitatively determined.

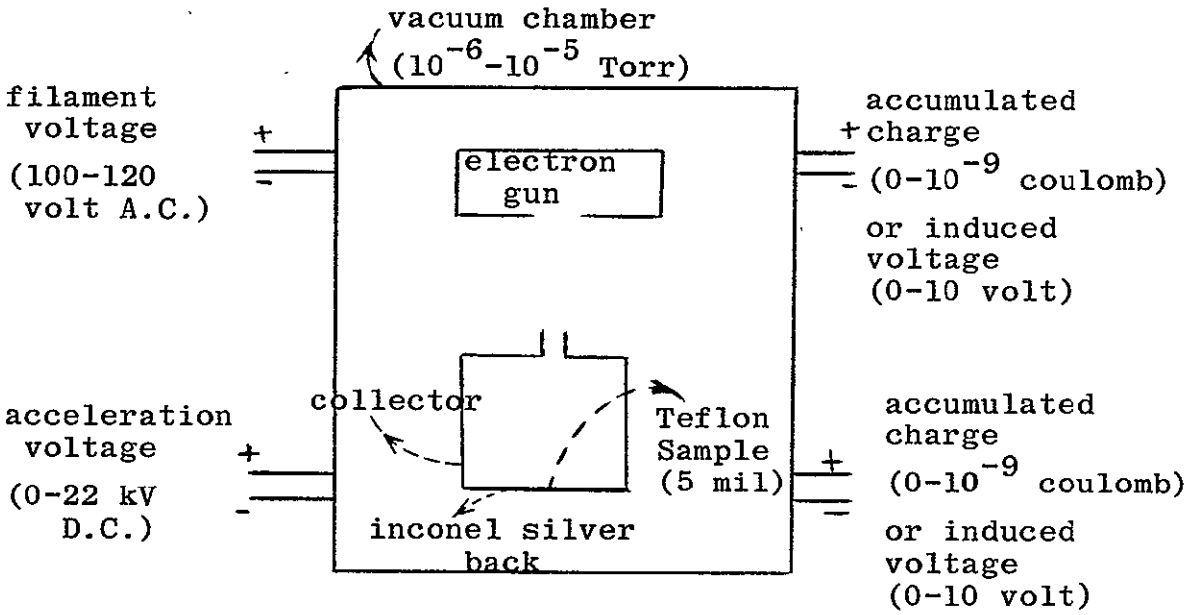

Figure (V-1) A schematically equivalent portrayal for the experiment. The parenthesized numbers are ranges in which we operated.

Two objectives were achieved via two methods. Method 1 [16] with many small-rectangular segments yields an accumulated charge (or voltage) distribution across the sample. From this distribution we solved a boundary-value problem. With the aid of a computer, numerical values of potential and field above the sample were found. As a continuation of the work, method 2 with a sample having a single-circular segment was used to measure the secondary electron emission from the sample's surface which was exposed to these fields and the fields enforced by the screen's presence. Information about the emission is conveyed from the collector and the underlying plane sample to the graphs on the recording chart by the induced currents on them. The interpretation requires mathematical manipulations and computer programming.

The apparatus employed in method 2 is that employed in method 1 with some modifications. However, the rectangularly segmented sample which is hard to fabricate becomes unnecessary for the secondary-electron emission measurements. In contrast, method 2 is inapplicable for charge measurements near the edges of the sample, because the narrowed beam would be largely deflected when it is directed toward them.

In order to see what the field patterns and equipotential contours look like in the vicinity of dielectric samples where charge accumulation appears, two different geometries were investigated. One was a sample under two rectangular apertures separated by a hemicylinder. In

accordance with experimental results, and for mathematical convenience, voltage distribution on either sample's surface could be treated as a function of one variable.

The potential everywhere in the upper-half space limited by the specimen satisfies Laplace's equation with Dirichlet boundary conditions. Applications of Green's theorem and Green's function simplify the solution significantly. The consequent potential and field are integral expressions of two variables. These analytic expressions combined with a so-called "trace the field" concept are powerful for numerical purposes. Fundamentally, tracing the field is performing a sequence of steps in the correct directions, parallel or perpendicular to the field at each point, under the control of certain convergence standards.

A computer subroutine (in Appendix A3), which implements the Green's solution for the Dirichlet boundary value problem and the concept of tracing the field, was written. It linearly interpolates a discrete set of boundary-potential points on the x-axis of a plane where potential is unchanging along the other axis. Then it produces equipotential contours and field patterns above that plane. The equipotentials and fields are functions of x and of the vertical variable in the three-dimensional space. Conformal transformations enable this subroutine to spread its usefulness to any electrostatic problem whose boundaries can be mapped into a plane. The two restrictions are that the potential

varies with only one variable on the plane and the contours must start from the plane.

In the measurement of secondary-electron emission from the dielectric sample by a probing beam when the sample had been already charged up by a charging beam, two phases were involved. The first phase was a strategy of distinguishing between primary electrons striking the sample and secondary electrons reaching the collector. Then the electron induced currents, amplified with the electrometers, were registered simultaneously on a recording chart. The second phase was merely the solving of an inverse-filtering problem. The forcing function to be specified is the current signal induced on the collector. The circuit is a simple parallel RC filter. The secondary-electron emission coefficient is the ratio of the maximal-secondary-electron-induced current to the constant-primary-electron-induced currents. In brief, the general behavior of the coefficient with respect to beam voltage in this experiment is analogous to the result accomplished by many other authors as shown in Fig. (V-2). More rigorously, as we should perceive, some factors associated with the secondary-electron emission do vary with an electric field.

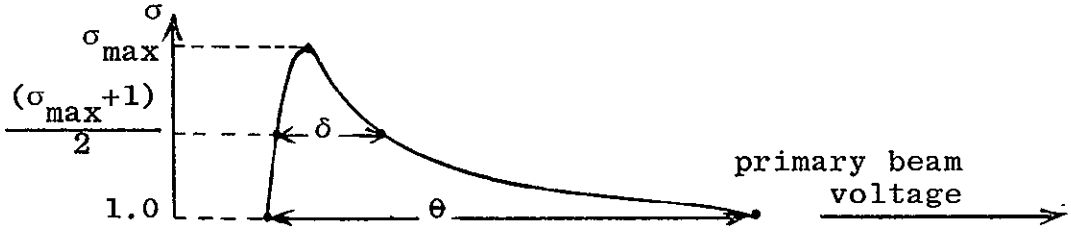

Figure (V-2) An ordinary curve for σ with factors: σ_{max}, δ, and θ.

With the screen's presence, it is obvious that the closer to the sample the screen is the stronger the field existing on the sample's surface becomes. Even though we were unable to ascertain precise values for the fields, comparisons shown in Fig. (IV-2)-Fig. (IV-6) among the threshold voltage intervals θ, among the peak values σ_{max}, and among the deviations δ do confirm the following statements:

a) The threshold voltage (surface potential), at which the number of primary electrons equal the number of secondary electrons, is smaller for a larger field. Therefore, the threshold interval θ, the voltage distance between two unit-σ points, is larger for a greater field.

b) Secondary-electron emission coefficient σ is a sharply increasing function with respect to primary voltage when it is slightly greater than the threshold voltage. We, therefore, may find more precise values of σ_{max} with a finer division in the primary beam. Anyway, the values of σ_{max} become low for a high field except at three data points where we presume that errors were made during the measurement and the calculation.

c) Without the field, the coefficient σ decreases 70% with a 50-volt shift to the left and 40% with a 50-volt shift to the right of the primary voltage from the voltage corresponding to peak value σ_{max} of the σ curve. In the presence of the strong field these percentages approach 20%

and 10%, respectively. In other words, if we call deviation δ the voltage interval between two points on the σ-curve at which σ decreases a half with respect to unity from its maximal value, then the deviation δ is larger with an influence of a stronger field.

Results from the computation in Chapter III reveal that the x-component of the field does not change much relatively compared to the y-component from one point to another across the sample, and that the x-component intensively dominates the y-component at field points near the edge. This revelation is merged with conclusions in a), b) and c) to deduce an explanation why the surface (threshold) potential dies off abruptly near the metal-dielectric interface. If we assume that the tangential field has an influence on secondary electron emission similar to the normal field, then we may conclude that because the steep gradient exists in the border, the threshold voltage must be low. The accumulated electrons are always motivated by this field to move to the edge. Therefore, the secondary electron emission (obviously, with the coefficient being reduced but greater than unity) is readily excited even at low surface potentials by the charging beam. Consequently, the gradient is maintained by a balance of the charge transfer process of secondary-electron emission with the primary electron beam. This discussion is consistent with the pattern of charge accumulation on a dielectric sheet which was firstly seen in the experiment, but was not explained.

APPENDIX A

A1 Proofs of Expression

1. Solution of Dirichlet problem with Green's function

Starting from the Green's theorem:

$$\int_V (\phi\nabla^2\psi - \psi\nabla^2\phi)\,dv = \oint_S \left[\phi \frac{\partial\psi}{\partial n} - \psi\frac{\partial\phi}{\partial n}\right] ds ,$$

a person is able to convert the Poisson differential equation, $\nabla^2\phi = -4\pi\rho$, into an integral equation if he chooses a particular ψ, namely Green's function $G(\vec{v},\vec{v}') = 1/|\vec{v};\vec{v}'|$ where $\vec{v}$ is the observation point and $\vec{v}'$ is the integration variable. Further, we put $\phi=\Phi$, a scalar potential, and make use of $\nabla^2 G(\vec{v};\vec{v}') = -4\pi\delta(\vec{v}-\vec{v}')$, so that the theorem becomes,

$$\int_V \Big[-4\pi\Phi(\vec{v}')\,\delta(\vec{v}-\vec{v}') + 4\pi\rho(\vec{v}')G(\vec{v};\vec{v}')\Big]dv' = \oint_S \Big[\Phi(\vec{v}')\frac{\partial}{\partial n'}G(\vec{v};\vec{v}') - G(\vec{v};\vec{v}')\frac{\partial\Phi}{\partial n'}(\vec{v};\vec{v}')\Big] ds' .$$

If the point $\vec{v}$ lies outside the surface (S), $\Phi(\vec{v}) = 0$. If $\vec{v}$ lies within the volume (V), then the equation becomes:

$$\Phi(\vec{v}) = \int_V \rho(\vec{v}')G(\vec{v};\vec{v}')dv'$$

$$+ \frac{1}{4\pi}\oint_S [\Phi(\vec{v}')\frac{\partial}{\partial n'}G(\vec{v};\vec{v}')$$

$$- G(\vec{v};\vec{v}')\frac{\partial\Phi}{\partial n'}(\vec{v};\vec{v}')]ds' \quad .$$

Two remarks are in order about the resulting expression $\Phi(\vec{v})$. First, if the surface (S) is at infinity and the electric field on (S) falls off faster $1/|\vec{v}-\vec{v}'|$, then the surface integral vanishes. Second, for a charge free volume the potential anywhere inside the volume is expressed in terms of the surface potential and its normal derivative.

The solution of the Poisson or Laplace equation in a volume (V) with either Dirichlet or Neumann boundary conditions on the boundary surface (S) can be simplified by choosing an appropriate $G(\vec{v};\vec{v}') = 1/|(\vec{v}-\vec{v}')|+F(\vec{v};\vec{v}')$, where $\nabla^2 F(\vec{v};\vec{v}') = 0$, to eliminate one or the other of the two surface integrals. For Dirichlet boundary conditions we demand that $G(\vec{v};\vec{v}')$ be zero when $\vec{v}'$ on (S). Then the solution is:

$$\Phi(\vec{v}) = \int_V \rho(\vec{v}')G(\vec{v};\vec{v}')dv'$$

$$- \frac{1}{4\pi}\oint_S \Phi(\vec{v}')\frac{\partial G}{\partial n'}(\vec{v};\vec{v}')ds' \quad .$$

We had a charge free volume such that the first term vanishes.

2. Complex transformations for field components

Let the variable $z = x+jy$ relate to $w = u+jv$ by $z=f(w)$, where f is the transformation from the z-plane to the w-plane. Let the function γ be given by $\gamma = \phi+j\psi$, where ϕ is potential and ψ is flux. Since ϕ and ψ are analytic function of (x,y) and therefore, of (u,v), the Cauchy-Riemann conditions permit the following manipulations:

$$E_x = -\left.\frac{\partial\phi}{\partial x}\right|_y = -\left.\frac{\partial\psi}{\partial y}\right|_x \; ; \quad E_y = -\left.\frac{\partial\phi}{\partial y}\right|_x = \left.\frac{\partial\psi}{\partial x}\right|_y \; ,$$

and

$$E_u = -\left.\frac{\partial\phi}{\partial u}\right|_v = -\left.\frac{\partial\psi}{\partial v}\right|_u \; ; \quad E_v = \left.\frac{\partial\phi}{\partial v}\right|_u = \left.\frac{\partial\psi}{\partial u}\right|_v \; .$$

Let's consider

$$\left.\frac{\partial\gamma}{\partial u}\right|_v = \frac{\partial\phi}{\partial u} + j\frac{\partial\psi}{\partial u} = -E_u+jE_v \; ,$$

and

$$\left.\frac{\partial\gamma}{\partial x}\right|_y = \frac{\partial\phi}{\partial x} + j\frac{\partial\psi}{\partial x} = -E_x+jE_y \; .$$

Then $\partial\gamma/\partial u$ can be written in terms of E_x, E_y and the derivative of the transformation as follows:

$$\left.\frac{\partial\gamma}{\partial u}\right|_v = \frac{1}{2}\left[\frac{\partial\gamma}{\partial x}\cdot\frac{\partial x}{\partial u} + \frac{\partial\gamma}{\partial y}\cdot\frac{\partial y}{\partial u}\right]$$

$$= \frac{1}{2}\left[(-E_x+jE_y)\frac{\partial}{\partial u}\mathrm{Re}\{z\} + (-E_y-jE_x)\frac{\partial}{\partial u}\mathrm{Im}\{z\}\right] \; .$$

Equating the real parts and imaginary parts of the two equations of $\partial\gamma/\partial u$, we construct the expression as used.

A2 Tabulated Formulae

1. Integrals [20]

$$\int \frac{x\,dx}{a+bx^2} = \frac{1}{2b} \ln(a+bx^2)$$

$$\int \frac{x\,dx}{(a+bx^2)^{m+1}} = \frac{-1}{2bm(a+bx^2)^m} \quad \text{for } m \geq 1$$

$$\int \frac{x^2\,dx}{(a+bx^2)^{m+1}} = \frac{-x}{2mb(a+bx^2)^m} + \frac{1}{2mb}\int \frac{dx}{(a+bx^2)^m}$$

$$\int \frac{dx}{a^2+b^2x^2} = \frac{1}{ab} \tan^{-1} \frac{bx}{a}$$

$$\int \frac{x\,dx}{(a+bx)^2} = \frac{1}{b^2} \left[\ln(a+bx) + \frac{a}{a+bx}\right]$$

These were used to evaluate the integrals of $P(x,y)\ E_x(x,y)$ and $E_y(x,y)$ in Chapter III.

2. Green's function [4]

For z-independent three-dimensional space, the Green's function has the form:

$$G(\vec{v};\vec{v}') = -2 \ln(|\vec{v}-\vec{v}'|/|\vec{v}'|), \quad \text{where}$$

$\vec{v} = (x,y)$ and $\vec{v}' = (x',y')$.

3. Conformal mapping [19]

a) $w = f(z) = \frac{1}{\pi}[s+\ln(s+z)]$, $s = \sqrt{z^2-1}$

b) $w = f(z) = z+1/z$.

A3 Computer Programs -- Limitations of the Generalized Computer Program

Generally, this program is able to find the equipotential contours and field components of any configuration which can be converted into a two-dimensional space where the boundary voltage on the horizontal x-axis is well-specified in the form of Fig. (III-3). Nevertheless, in order to use it efficiently one should learn several features of its structure.

The two main programs were used to call subroutine Green (below) in Chapter III are:

1. Main Program 1

```
      COMMON /ORI/ C(30), V(30), BE(30), AL(30), PY, NN
      COMMON /ARR/ XG(10,50),YG(10,50),FX(10,50),FY(10,
          50),PP(10),KK(10)
      READ (5,1) N, NPOTEN, NPOINT, PMIN, PSTEP,ADJ
    1 FORMAT (3I5,4F10.0)
      PY = 3,1415926
      NN = N - 1
      DO 10 I = 1, N
         READ (5,2) COOR,V(I)
    2    FORMAT(2F20.0)
      C(I) = TRNSFM(PY,COOR)
         WRITE(6,3) V(I),COOR,C(I)
    3    FORMAT(1H ,3(20X,E13.5) )
   10 CONTINUE
```

```
      CALL GREEN (M,NPOTEN,NPOINT,PMIN,PSTEP,ADJ)
      DO 101 I = 1, M
               WRITE (6,4) PP(I)
    4       FORMAT (///,20X,'P = ',1(E13.5,20X)///20X,
     'ABSS',26X,'ORDI',26X,'EX',28X,'EY'///)
      IF ( KK(I) .LT. 0 ) KK(I) = -KK(I)
         JJ = KK(I)
      DO 102 J = 1, JJ
               CALL INVRS1 (PY,XG(I,J),YG(I,J),X,Y)
      IF ( J .EQ. 1 ) GO TO 103
               CALL INVRS2 (PY,X,Y,FX(I,J),FY(I,J),EX,EY)
               WRITE (6,6) X, Y, EX, EY
    6          FORMAT (1H ,4(17X,E13.5) )
      GO TO 102
  103         WRITE (6,6) X, Y
  102    CONTINUE
      IF ( KK(I) .LT. 0 ) PRINT 7
    7 FORMAT(/20X,'SUBPROGRAM SCAN COULD NOT FIND THE
     1,SUCCESSIVE POINT')
  101 CONTINUE
      STOP
      END

      FUNCTION TRNSFM(PY,W)
      Z = 1.2
      IF ( W .EQ. 0.0 ) Z = 1.0
      DO 30 I = 1, 30
      F = (1/PY) * (SQRT(Z**2-1)+ ALOG(Z + SQRT(Z**2 - 1)))
     1, - W
      IF ( ABS(F) .LE. 1.0E-7 ) GO TO 101
      G = (1/PY) * ( (Z+1)/SQRT(Z**2-1) )
         ZIT = Z - F / G
      IF ( ABS(ZIT-Z) .LE.  1.0E-7 ) GO TO 100
      Z = ZIT
      IF ( ZIT .LE. 1.0 ) ZIT = ( (Z-1)/2 + Z )
   30 CONTINUE
  100 TRNSFM = ZIT
      RETURN
  101 TRNSFM = Z
      RETURN
      END

      SUBROUTINE INVRS1 (PY,ABSS,ORDI,X,Y)
      COMPLEX U, Z, W
      Z = CMPLX(ABSS,ORDI)
        U = CSQRT( CMPLX((ABSS**2-ORDI**2-1),(2*ABSS*ORDI)) )
      IF ( ABSS .LT. 0.0 ) U = -U
      W = (1/PY) * ( U + CLOG(Z+U) )
      X = REAL(W)
      Y = AIMAG(W)
      RETURN
      END
```

```
      SUBROUTINE INVRS2 (PY,X,Y,FX,FY,EX,EY)
      COMPLEX Z
      Z = CSQRT( CMPLX((X**2+Y**2-1),-2*Y) ) / SQRT((X-1)
     1 **2+Y**2)
      G = REAL(Z) / PY
      H = AIMAG(Z) / PY
      EX = FX*G + FY*H
      EY = -FX*G + FY*G
      RETURN
      END
```

2. Main Program 2

```
      COMMON /ORI/ C(30), V(30), BE(30), AL(30), PY, NN
      COMMON /ARR/ XG(10,50),YG(10,50),FX(10,50)FY(10,50)
     1,PP(10),KK(10)
      W(Z) = Z + 1 / Z
      READ (5,1) N, NPOTEN, NPOINT, PMIN, PSTEP,ADJ
    1 FORMAT (3I5,4F10.0)
      WRITE(6,8)
    8 FORMAT(///,21X,'ABCISSA',15X,'MODIFIED ABCISSA',25X
     1,'POTENTIAL',///)
      NN = N - 1
      DO 10 I = 1, N
           READ (5,2) COOR,V(I)
    2      FORMAT(2F20.0)
      C(I) = W(COOR)
      WRITE(6,3) COOR,C(I),V(I)
    3   FORMAT(1H ,3(20X,E13.5) )
   10 CONTINUE
      CALL GREEN (M,NPOTEN,NPOINT,PMIN,PSTEP,ADJ)
      IF ( M .EQ. 0 ) STOP
      DO 101 I = 1, M
                WRITE (6,4) PP(I)
    4         FORMAT (///,20X,'P = ',1(E13,5,20X)///20X,
     1,'ABSS',26X,'ORDI',26X,'EX',28X,'EY'///)
          JJ = KK(I)
      IF(KK(I) .LT. 0 ) JJ = -JJ
      DO 102 J = 1, JJ
      IF(J.EQ.1) GO TO 103
      CALL INVERS(  XG(I,J),YG(I,J),FX(I,J),FY(I,J),X,Y,
     1,EX,EY)
                WRITE (6,6) X, Y, EX, EY
    6           FORMAT (1H ,4(17X,E13.5) )
      GO TO 102
  103 CALL INVERS( XG(I,1),YG(I,1),0.,0.,X,Y,EX,EY)
      WRITE(6,6) X,Y
  102    CONTINUE
      IF ( KK(I) .LT. 0 ) PRINT 7
    7 FORMAT(/20X,'SUBPROGRAN SCAN FAILED TO CONVERGE FOR
     1 NEXT POINT')
  101 CONTINUE
      STOP
      END
```

```
      SUBROUTINE INVERS(U,V,EU,EV,X,Y,EX,EY)
      COMPLEX Z, W, S
      W = CMPLX(U,V)
      S = CSQRT(W**2 - 4)
      IF ( U .LT. 0.0 )  S = -S
      P = REAL(S)
      Q = AIMAG(S)
      Z = ( W + S ) / 2
      X = REAL(Z)
      Y = AIMAG(Z)
      G = ( X*P + Y*Q ) / ( P**2 + Q**2 )
      H = ( Y*P - X*Q ) / ( P**2 + Q**2 )
      EX = EU*G + EV*H
      EY = -EU*H + EV*G
      RETURN
      END
```

The user must supply a data card to be read with the format (3I5,3F10.0) and containing the following:

N: Number of data points not larger than 30,

NPOTEN: Number of contours not larger than 10,

NPOINT: Number of points on each contour not larger than 50,

PMIN: The first potential value among the contours to be calculated,

PSTEP: The algebraic separation (potential-dimension) between contours,

ADJ: Adjustment factor ranging approximately from 0.1 to 1. The larger it is the greater the separation of two successive points on one contour becomes.

The user must also supply N data cards (2F20.0) having the entries:

x'(I), V(I): Boundary coordinates and voltages on the straight line (u-axis in w-plane).

3. Subroutine GREEN

```
      SUBROUTINE GREEN (M,NPOTEN,NPOINT,PMIN,PSTEP,ADJ)
      COMMON /ARR/ XG(10,50),YG(10,50),FX(10,50),FY(10,
     1,50),PP(10),KK(10)
      COMMON /ORI/ C(30), V(30), BE(30), AL(30), PY, NN
      FY = 3,1415926
      DO 11 I = 1, NN
         BE(I) = ( V(I+1) - V(I) ) / ( C(I+1) - C(I) )
      AL(I) = V(I) - BE(I) * C(I)
   11 CONTINUE
      M = 0
      DO 12 I = 1, NPOTEN
         KEY = 0
         P = PMIN + (I-1) * PSTEP
         DO 13 J = 1, NN
      IF ( M .EQ. 10 ) RETURN
         ORDI = 0.0
            IF ( (P-V(J))*(P-V(J+1)) ) 131, 132, 13
  131 ABSS = (P-V(J)) * (C(J+1)-C(J)) / (V(J+1)-V(J))+C(J)
      GO TO 130
  132       IF( P .EQ. V(J) ) GO TO 133
      GO TO 13
  133       ABSS = C(J)
  130 M = M + 1
      KEY = 1
      SNS = - SIGN(ADJ,BE(J))
      KK(M) = NPOINT
      PP(M) = P
            XG(M,1) = ABSS
            YG(M,1) = ORDI
            ORDI = ABS(C(J+1)-C(J)) / 200.0
            DO 14 K = 2, NPOINT
               CALL SCAN ( P,PSTEP,BE(J),ABSS,ORDI,EX,EY,
     1 E2,KASE )

      IF (KASE) 142,141,142
  141 XG(M,K) = ABSS
      YG(M,K) = ORDI
      FX(M,K) = EX
      FY(M,K) = EY
                ABSS = ABSS - SNS*ABS(PSTEP)*EY/E2
                ORDI = ORDI + SNS*ABS(PSTEP)*EX/E2
      IF(ORDI.LE.0.) KK(M) = K
                IF (ORDI) 13, 13, 14
  142 KK(M) = (K-1) * KASE
                GO TO 13
   14       CONTINUE
   13    CONTINUE
            IF ( KEY .EQ. 0 ) WRITE(6,7)  P
    7 FORMAT(//20X,'THERE IS NO CONTOUR CORRESPONDING TO
     1'P = ',E13.5//)
```

```
12 CONTINUE
   RETURN
   END

   SUBROUTINE SCAN (P,PSTEP,BE,X,Y,EX,EY,E2,KASE)
   DO 40 I = 1, 50
      EX = FIELDX (X,Y)
      EY = FIELDY (X,Y)
      E2 = EX**2 + EY**2
      TEST = BE**2 * 1.0E-6
      IF ( E2 .LT. TEST ) GO TO 44
      DIF = POTEN (X,Y) -  P
      CRI = ABS(PSTEP) * 1.0E-4
      IF ( ABS(DIF) .LE. CRI ) GO TO 42
      X = X + DIF*EX/E2
      Y = Y + DIF*EY/E2
   IF(Y,LE.0.) GO TO 44
40 CONTINUE
   KASE = -1
   RETURN
42 KASE = 0
   RETURN
44 KASE = 1
   RETURN
   END

   FUNCTION POTEN(X,Y)
   COMMON /ORI/ C(30), V(30), BE(30), AL(30), PY, NN
   R(T) = (1/PY) * ATAN2(T-X,Y)
   S(T1,T2) = (0.5*Y/PY) * ALOG( (Y**2+(T2-X)**2)
  1,/(Y**2+(T1-X)**2) )
   N = NN + 1
   POTEN = 0.5 * ( V(1) + V(N) ) + V(1) * R(C(1)) -
  1, V(N) * R(C(N))
   DO 20 I = 1, NN
20 POTEN = POTEN + ( BE(I)*X + AL(I) ) * ( R(C(I+1)) -
  1, R(C(I)) ) + BE(I) * S(C(I),C(I+1))
   RETURN
   END

   FUNCTION FIELDX(X,Y)
   COMMON /ORI/ C(30), V(30), BE(30), AL(30), PY, NN
   R(T) = (1/PY) * ATAN2(T-X,Y)
   S1(T) = (Y/PY) / (T-X)**2 + Y**2 )
   S2(T) = (T-X) * S1(T)
   N = NN + 1
   FIELDX = V(1) * S1(C(1)) - V(N) * S1(C(N))
   DO 30 I = 1, NN
30 FIELDX = FIELDX + ( BE(I)*X + AL(I) ) * ( S1(C(I+1))
  1  - S1(C(I)) ) + BE(I) * ( S2(C(I+1)) - S2(C(I))
  2  - R(C(I+1)) + R(C(I)) )
   RETURN
   END
```

```
      FUNCTION FIELDY(X,Y)
      COMMON /ORI/C(30), V(30), BE(30), AL(30), PY, NN
      R1(T) = ( (T-X)**2 + Y**2 )
      R2(T) = (T-X) / R1(T)
      S(T1,T2) = 0.5 * ALOG( R1(T2) / R1(T1) )
      N = NN + 1
      FIELDY = V(1) * R2(C(1)) - V(N) * R2(C(N))
      DO 35 I = 1, NN
   35 FIELDY = FIELDY + ( BE(I)*X + AL(I) ) * ( R2(C(I+1))
     1  - R2(C(I)) ) - BE(I) * ( Y**2 * (1/R1(C(I+1))
     2  -1/R1(C(I))) + S(C(I),C(I*1)) )
      FIELDY = FIELDY / PY
      RETURN
      END
```

Subroutine GREEN is the implementation of Eqns. (III-1) to (III-9) and the process described in Section B. This subroutine references three other subprograms that provide potential and field components at a particular point. After GREEN is executed, there are four two-dimensional arrays and two one-dimensional arrays in the block COMMON |ARR| available for printing or further operations. The argument M in the CALL statement indicates the number of contours which GREEN has found where $0 \leq M \leq 10$. GREEN "there is no contour corresponding to P" when it cannot be found. The array contents are as follows:

XG(I,J): x coordinates of the J^{th} point, I^{th} contour on the z plane,

YG(I,J): y coordinates of the J^{th} point, I^{th} contour on the z plane,

FX(I,J): x component of the field at (XG(I,J), YG(I,J)),

FY(I,J): y component of the field at (XG(I,J), YG(I,J)),

REFERENCES

1. Austin, L. and H. Starke. Uber die Reflection der Kathodenstrahlen und Eine Damit Verbundene Neuve Ercheinung Sekundarer Emission. Ann. Phys. Lpz., 1902, 9, p. 271.

2. Jenkins, R. O. and W. G. Trodden. Electron and Ion Emission from Solids. Dover Publications, Incorporated, 1965, pp. 54-70.

3. McKay, K. G. Secondary Electron Emission, Advances in Electronics, New York, 1948, I, p. 166.

4. Bruining, H. Secondary Electron Emission, Part III. Secondary Electron Emission Caused by Bombardment with Slow Primary Electrons. Physica, Haag, 5, p. 913.

5. Bruining, H. M. B. E. Physics and Applications of Secondary Electron Emission. McGraw-Hill Book Company, Incorporated, 1954.

6. Jonker, J. L. H. On the Theory of Secondary Electron Emission. Phillips Res. Repts., 7, p. 1.

7. Baroddy, E. M. A Theory of Secondary Emission from Metals. Phys. Rev., 78, p. 780.

8. Kadyschevitch, A. E. Theory of Secondary Emission from Metals. J. Phys. USSR, 2, p. 115.

9. Baroody, E. M. Application of Wooldridge Theory of Secondary Emission. Phys. Rev., 83, 857.

10. Frohlich. Theorie der Sekundarelecktronenemission von Metallen. Ann. Phys. Lpz., 13, p. 229.

11. Wooldridge, D. E. Theory of Secondary Emission. Phys. Rev., 56, p. 562.

12. Dekker, A. J. and A. Van Der Ziel. Theory of the production of Secondary Electron in Solids. Phys. Rev., 86, p. 755.

13. Wall, J. A., E. A. Burke, and A. R. Frederickson. Results of Literature Search on Dielectric Properties and Electron Interaction Phenomena Related to Spacecraft Charging. Dupty for Electronic Technology (RADC). Solid State Science Division, Hanscom AFB, MA 01731.

14. Matskevich, T. L., Secondary Electron Emission of Some Polymers. Fiz. Tverd. Tela, Akad, Nauk, 1959 USSR 1, p. 277.

15. Robinson, James W. Surface Charge Kinetics near Metal-Dielectric Interfaces Exposed to Kilovolt Electron Flux. Final Report, September, 1977, NASA Grant No. NSF-3097.

16. Robinson, James W. Surface Charge Kinetics near Metal-Dielectric Interfaces Exposed to Kilovolt Electron Flux. Semi-annual Progress Report, August 1976, NASA Grant No. NSF-3097.

17. Jackson, John David. Classical Electrodynamics. 2nd edition. John Wiley and Sons, Incorporated, 1975, pp. 40-44.

18. Morse, Phillip M. and Herman Fesbach. Methods of Mathematical Physics. McGraw-Hill Book Company, Incorporated, 1953, pp. 812-813.

19. Churchill, Ruell V. Complex Variables and Applications. McGraw-Hill Book Company, Incorporated, 1974, pp. 320-324.

20. Beyer, William H. Standard Mathematical Tables. 24th edition. CRC Press, Incorporated, 1976, pp. 339-342.